Theory of Surface Micelles of Semifluorinated Alkanes

ARTICLE *in* LANGMUIR · NOVEMBER 2006

Impact Factor: 4.46 · DOI: 10.1021/la060638+ · Source: PubMed

4 AUTHORS, INCLUDING:

Alfredo Gonzalez-Perez
University of Copenhagen
77 PUBLICATIONS **1,049** CITATIONS
SEE PROFILE

Marie Pierre Krafft
University of Strasbourg
169 PUBLICATIONS **3,478** CITATIONS
SEE PROFILE

Theory of Surface Micelles of Semifluorinated Alkanes

Alexander N. Semenov,* Alfredo González-Pérez, Marie Pierre Krafft, and Jean-François Legrand

Institut Charles Sadron, 6 rue Boussingault, 67083 Strasbourg Cedex, France

Received March 8, 2006. In Final Form: June 13, 2006

Surface structures of semifluorinated alkanes $F(CF_2)_n(CH_2)_mH$ (referred to as FnHm) spread on the air/water interface are investigated theoretically. The study is focused on the disklike surface micelles that were recently identified by AFM and scattering techniques at sufficiently high surface concentrations. We show that (1) the micelles emerge as a result of liquid/liquid (rather than liquid/gas) phase separation in the Langmuir layer; (2) the micelles are islands of the higher-density phase with roughly vertical orientation of FnHm molecules (F-parts extend toward air, H-parts toward water) and the matrix is the lower density-phase where the FnHm diblocks are nearly parallel to the water surface; (3) the micelles and the hexagonal structure they form are stabilized by the electrostatic interactions which are mainly due to the vertical dipole moments of the CF_2- CH_2 bonds in the vertical phase; and (4) the electrostatic repulsive interactions can serve to suppress the micelle size polydispersity.

1. Introduction

It is well-known that amphiphilic molecules in solution (like surfactants or block copolymers) often tend to form aggregates of well-defined size, i.e., micelles.[1−6] Similar aggregates in two dimensions (surface micelles) are much less investigated.[7−15] The micelle size is normally of the order of (or less than) the length of the amphiphilic molecules. For example, the radius of spherical block-copolymer micelles in the bulk (which are 3-dimensional analogues of disklike surface micelles) is always smaller than the total molecular length.[2−4] In this paper, we consider an anomalous system involving large surface micelles: their diameter is much larger (by 1 order of magnitude) than the molecular size. We focus on the relatively novel surface micelles formed by semifluorinated alkanes $C_nF_{2n+1}C_mH_{2m+1}$ (FnHm) in Langmuir monolayers.[7,8] The introduction of a perfluoroalkylated fragment (F_n stands for C_nF_{2n+1}) in a molecule results in its enhanced amphiphilic character. F chains and F amphiphiles, as compared to standard hydrocarbon amphiphiles, are characterized by lower surface tensions, higher hydrophobicity (and higher affinity for gases), and a much stronger tendency to self-aggregation.[16,17]

The most important features of micelles formed by FnHm molecules on the water/air interface are summarized below:

(1) The FnHm amphiphilic molecules are special as both F and H blocks tend to avoid contact with water. Additionally, the F and H blocks tend to avoid each other. Altogether, the FnHm molecules attract each other and form Langmuir monolayers. X-ray reflectivity measurements[7,8,18,19] show that the thickness of the F8H16 monolayer is around 3 nm. This thickness can be compared with the total length of the F8H16 molecule, $l \approx 3.3$ nm. The structure of the FnHm layers is a controversial issue[7,8,18,19] to be discussed in this paper.

(2) The Langmuir films of F8H16 often show molecular patterns involving nearly circular domains. The micelle diameter of $D \approx 30$ nm was obtained by both AFM studies of the F8H16 monolayers transferred onto silicon wafers and by small-angle X-ray scattering (GISAXS) of the original F8H16 monolayers at the water/air interface.[7,8,12] The domains formed by F8H16 are therefore much larger than the typical size of low-molecular-weight surfactant surface micelles (∼5 nm, i.e., of the order of the surfactant's molecular length[14]).

The present paper is focused on structures of semifluorinated alkanes involving disklike surface micelles. A range of other surface structures with noncircular domains of FnHm was also observed.[7,8,10] These structures are discussed in section 7 (point 15).

(3) The arrangement of the micelles depends on surface pressure P_s. At high P_s ($\gtrsim$0.5 dyn/cm; note that dyn/cm = mN/m), the micelles form ordered hexagonal arrays and are rather monodisperse.[7,8,12] At lower P_s ($\lesssim$0.5 dyn/cm), the micelles are less ordered based on the AFM images of the transferred films (see below, Figures 2 and 3).

(4) The surface micelles of F8H16 have been seen at $P_s \gtrsim 0.5$ dyn/cm as soon as measurements have started (∼15 min after

* To whom correspondence should be addressed.

(1) Elias, H.-G. The study of association and aggregation via light scattering. In *Light scattering from polymer solutions*; Huglin, M. B., Ed.; Academic Press: London, 1972; Chapter 9.
(2) Leibler, L.; Orland, H.; Wheeler, J. *J. Chem. Phys.* **1983**, *79*, 3550.
(3) Halperin, A. *Macromolecules* **1987**, *20*, 2943.
(4) Marques, C. M.; Joanny, J. F.; Leibler, L. *Macromolecules* **1988**, *21*, 1051.
(5) Shim, D. F. K.; Marques, C. M.; Cates, M. E. *Macromolecules* **1991**, *24*, 5309.
(6) Nyrkova, I. A.; Semenov, A. N. *Eur. Phys. J. E* **2005**, *17*, 327.
(7) Maaloum, M.; Muller, P.; Krafft, M. P. *Angew. Chem., Int. Ed.* **2002**, *41*, 4331.
(8) Zhang, G.; Maaloum, M.; Muller, P.; Benoit, N.; Krafft, M. P. *Phys. Chem. Chem. Phys.* **2004**, *6*, 1566. Zhang, G.; Marie, P.; Maaloum, M.; Muller, P.; Benoit, N.; Krafft, M. P. *J. Am. Chem. Soc.* **2005**, *127*, 10412.
(9) Huang, Z.; Acero, A. A.; Lei, N.; Rice, S. A.; Zang, Z.; Schlossmann, M. L. *J. Chem. Soc., Faraday Trans.* **1996**, *92*, 545.
(10) Mourran, A.; Tartsch, B.; Gallyamov, M.; Magonov, S.; Lambreva, D.; Ostrovskii, B. I.; Dolbnya, I. P.; de Jeu, W. H.; Moeller, M. *Langmuir* **2005**, *21*, 2308.
(11) Maaloum, M.; Muller, P.; Krafft, M. P. *Langmuir* **2004**, *20*, 2261.
(12) Fontaine, P.; Goldmann, M.; Muller, P.; Faure, M. C.; Konovalov, O.; Krafft, M. P. *J. Am. Chem. Soc.* **2005**, *127*, 512.
(13) Cox, J. K.; Eisenberg, A.; Lennox, R. B. *Curr. Opin. Colloid Interface Sci.* **1999**, *4*, 52.
(14) Manne, S.; Schaffer, T. E.; Huo, Q.; Hansma, P. K.; Morse, D. E.; Stucky, G. D.; Aksay, I. A. *Langmuir* **1997**, *13*, 6382.
(15) Schneider, M. F.; Andelman, D.; Tanaka, M. *J. Chem. Phys.* **2005**, *122*, 094717.
(16) Riess, J. G. *Tetrahedron* **2002**, *58*, 4113.
(17) Krafft, M. P. In *Handbook of Fluorous Chemistry*; Gladysz, J. A., Curran, D. P., Horvath, I. T., Eds.; Wiley-VCH: Weinheim, Germany, 2004.
(18) El Abed, A.; Faure, M. C.; Pouzet, E.; Abillon, O. *Phys. Rev. E* **2002**, *65*, 051603.
(19) El Abed, A.; Pouzet, E.; Faure, M. C.; Saniere, M.; Abillon, O. *Phys. Rev. E* **2000**, *62*, 5895.

10.1021/la060638+ CCC: $33.50
Published on Web 09/13/2006

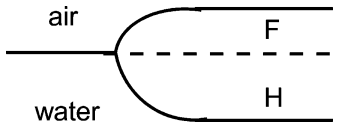

Figure 1. Tentative structure of the edge of a monolayer formed by FnHm molecules.

deposition of F8H16 on the water surface). Micelle diameter did not change, at a given P_s, throughout the observation period (up to 6 h in GISAXS experiments).

The aim of this paper is to try and rationalize how such large surface micelles can be stable. In the next section, we explain, basing on a simple phenomenological approach, why it is unlikely that a micelle is much larger than the size of the constituent molecules. We also discuss the proposed[7,8] disklike model for the surface micelles.

In section 3, we show that the picture of disklike micelles separated by regions of almost clean water surface, i.e., by the "surface gas" phase, is inconsistent with the experimental data. The model involving two liquid phases is then discussed. The structure of the two phases is considered in section 4. In particular, we point out that the electrostatic effects play an important role for the system as the F/H interfaces are likely to be electrically polarized. The resulting electrostatic interactions of micelles are quantitatively analyzed in section 5. The role of these interactions in the stabilization of micelles and their ordered patterns is considered in section 6. The main results are summarized and discussed in the last section.

2. Micelle Free Energy: A Phenomenological Approach

A Langmuir monolayer can be viewed as a condensed surfactant phase (for example, a 2-dimensional liquid) which can be in equilibrium with the surface gas phase (with negligible surface pressure) or can be further compressed by an external force. The important parameter is the energy λ of the liquid/gas interface, i.e., the edge tension of the layer (which is analogous to the surface tension of a 3-dimensional bulk liquid). A tentative edge structure of the Langmuir layer of FnHm surfactants is shown in Figure 1.

A continuous and macroscopic 2-dimensional liquid phase is stable if the edge is unfavorable, $\lambda > 0$. If $\lambda < 0$, then the edge length tends to increase, so that the layer tends to break into small pieces, either individual molecules (then the liquid is totally unstable) or micelles. To further explore the latter possibility, we take into account that the edge tension λ can depend on the edge curvature $C = 1/R$ (R = radius of curvature):

$$\lambda = \lambda(C) = \lambda_0 + \lambda_1 C + \lambda_2 C^2/2 + ...$$

The parameter λ_1 is nonzero since the two sides of the edge are not equivalent: the liquid phase (the Langmuir film) is on the one side and the surface gas phase is on the other side.

Let us *assume* that $\lambda_1 < 0$, meaning a tendency for a convex film edge. As for the magnitude of λ_1, it can be estimated in the following way: it is expected that the curvature significantly affects the tension λ if its radius is comparable with the thickness of the edge region, i.e., with the correlation length ξ in the film. Typically, $\xi \sim l$ (the molecular length), so $\lambda_0 \sim |\lambda_1|C$ for $C \sim 1/l$, i.e., $\lambda_0/|\lambda_1| \sim 1/l$. If disklike islands (of radius R) are formed instead of a continuous film, the edge free energy penalty per unit area of the film is

$$f = \frac{2\pi R\lambda(1/R)}{\pi R^2}$$

Minimizing f with respect to R (with $\lambda_0 > 0$, $\lambda_1 < 0$ and $\lambda_2 > 0$), we get $R < |\lambda_1|/\lambda_0 \sim l$. In the general case, we must therefore expect the micelle size to be of the same order as (or less than) the length of the surfactant molecules (if the micelles are formed at all). Large micelles are possible only if λ_0 (the energy of the straight edge) is anomalously small, for example, if λ_0 vanishes at some point, and in the vicinity of this point. However, it is hardly possible that the edge in Figure 1 may be characterized by a vanishing energy: the edge definitely involves an extra area of H/water interface (and, to a lesser extent, F/air interface), i.e., a considerable energy penalty (the tensions of F/air and H/water interfaces are around 20 dyn/cm and 30 dyn/cm, respectively). The observed large micelle size cannot therefore be explained just by the curvature dependence of the edge energy. In what follows, we will thus neglect this dependence since the edge curvature is small for large circular micelles.

A different interpretation was proposed in the pioneering papers[7,8] where the large FnHm surface micelles were reported. That argument was based on the density mismatch between F and H sublayers: if the F blocks are packed with the density typical of fluorocarbons in the bulk, the density in the H layer has to be considerably lower (by ~35%) than the corresponding bulk density. The argument, however, assumes that the H blocks are fully extended perpendicular to the layer, which may not be the case: if the H blocks are tilted at an angle around 45°, the density mismatch is compensated without resorting to micelle formation. The density mismatch can also be compensated with zigzag, or helical, or partially random-coil conformations of H blocks.

3. Surface Pressure and Ordering of Micelles

In this section, we turn more closely to the puzzle of large surface micelles. To begin with, let us analyze the available experimental data indicating how the FnHm micelle patterns evolve as a function of the exerted surface pressure P_s. The AFM studies[7,8] of the transferred F8H16 layers at $P_s = 5-7$ dyn/cm show that micelles of $D \approx 33$ nm (the accuracy is about 10%) are nearly closely packed in well-ordered hexagonal arrays. The micelles are disklike and are rather monodisperse. On the other hand, at $P_s = 0.5$ dyn/cm, the micelles apparently form a less ordered hexagonal structure with wider gaps between them and with more defects (Figure 2); the mean micelle diameter is $D \approx 26$ nm (i.e., it is smaller than at the higher P_s), and the mean intermicellar distance is larger ($D_{inter} \approx 35$ nm) than for the higher $P_s = 7$ dyn/cm. Thus, the micelle concentration at $P_s = 0.5$ dyn/cm is slightly lower (by ca. 12%) than that at $P_s = 7$ dyn/cm. The areas per molecule at $P_s = 7$ and 0.5 dyn/cm are $A = 0.30$ and 0.33 nm^2, respectively, the area difference being about 10%. The *total number* of micelles is therefore nearly independent of P_s: this number is virtually the same for $P_s = 0.5$ and 7 dyn/cm.

The direct small-angle X-ray scattering (GISAXS) of FnHm surfactants at the water/air interface essentially confirms the AFM picture.[12] The scattering curve obtained at 5 dyn/cm indicates a good hexagonal order; the lattice parameter (which must coincide with micelle diameter if they touch each other) is $D \approx 33.5$ nm. The hexagonal order persists at lower P_s (down to $P_s = 0.5$ dyn/cm); no diffraction peaks are observed at $P_s \approx 0$ ($A \approx 0.4$ nm^2). [Note that the accuracy of P_s measurements was about 0.1 dyn/cm, so $P_s \approx 0$ means $|P_s| \lesssim 0.1$ dyn/cm.] Nevertheless, our recent AFM experiments indicate that surface micelles are formed

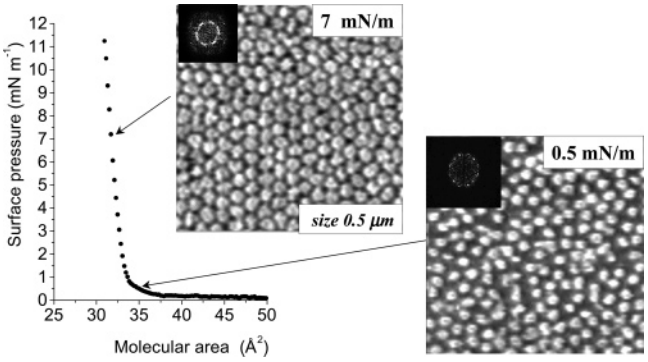

Figure 2. AFM images of the F8H16 films transferred onto silicon wafers at $P_s = 0.5$ dyne/cm (right) and $P_s = 7$ dyne/cm (left).[7]

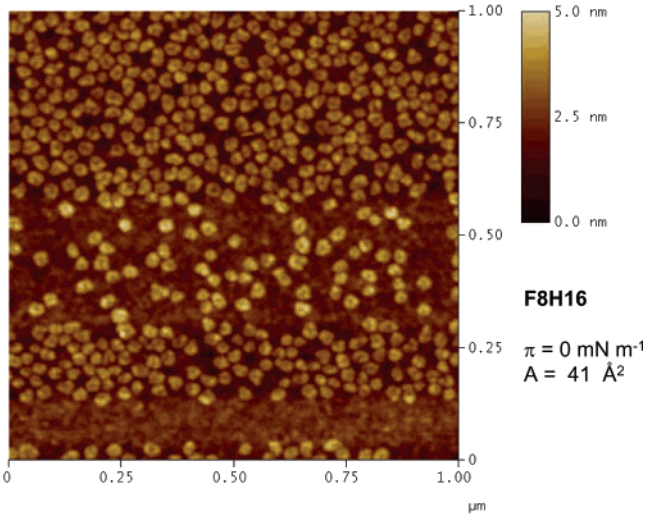

Figure 3. AFM images (1 μm × 1 μm) of a monolayer of F8H16 transferred onto a silicon wafers at $P_s \approx 0$ (area per molecule $A \approx 0.41$ nm^2). The monolayers were compressed up to the desired area on a Langmuir minitrough at 20 °C (Nima, total film area = 235 cm^2, compression rate = 20 cm^2/min, i.e., 0.07 nm^2/min per molecule) and transferred onto a silicon wafer using the LB technique (one monolayer transferred, lift speed of 1 mm/min). The transferred films were analysed with an atomic force microscope (NanoScope III) in tapping mode. The cantilever (Olympus) was fitted with a very sharp tip (5 nm).

also at $P_s \approx 0$ (see Figure 3). The micelles are not ordered well on the average at low $P_s \approx 0$ (more precisely, at $A \approx 0.41$ nm^2).

Thus, both AFM and X-ray data indicate that the FnHm surface micelles undergo an ordering transition (crystallization in a hexagonal network) at $P_s \lesssim 0.5$ dyn/cm. Are there any implications of this experimental result? Temporarily disregarding the issue about the mechanism of micelle formation, let us figure out the theoretical anticipation for $P_s = P^c$ at the crystallization transition. Two-dimensional systems of hard disks are well-studied by computer simulations. In the case of purely hard core (i.e., repulsive and short-range) interactions of disks, the liquid → hexagonal crystal transition is predicted at $P^c \approx 9\ (k_BT/D^2)$.[20] This gives $P^c \approx 0.05$ dyn/cm for $D = 26$ nm. It is important that any additional interactions between the disks (longer-range repulsion or attraction) would only decrease the theoretical pressure threshold. A polydispersity of disks can slightly increase the threshold pressure, but the effect is not too strong: a 20% increase of P^cD^2/k_BT was simulated for a system with the standard deviation of the disk diameter of 25%.[21] The area fraction of disks obtained in simulations at P^c is $\phi \approx 0.7$.

Although the experimental P^c is not known precisely enough, let us discuss two possibilities.

(1) If the experimental P^c is ~ 0.5 dyn/cm, then it would be much higher than the above theoretical estimate. It seems that the only reasonable way to get out of this contradiction is to assume that the surface pressure is not just due to the interactions between micelles. In other words, we have to assume that the gaps between the micelles are not clean water but rather they are also covered by the surfactant FnHm molecules. In this case, the surfactant film is continuous (albeit its thickness in the gaps is expected to be different from that inside micelles), and the surface pressure can be maintained by the intermolecular forces in the gaps.

(2) Alternatively, if we assume that the model of interacting disks (as in the simulations) is valid, then the crystallization transition must occur at $P_s \sim 0.05$ dyn/cm. The theoretical area fraction of micelles at the transition point is $\phi \sim 0.7$. Then, if this is true, the area fraction of micelles must be close to $\phi_{max} \approx 0.9$ at a much higher pressure $P_s \approx 0.5$ dyn/cm. However, the experimental ϕ at $P_s \approx 0.5$ dyn/cm is ≈ 0.50. What could be the reason for such a discrepancy? One possibility is that the interactions between micelles are not just hard-core, but rather are long-range. A long-range attraction of micelles would result in a larger ϕ at the transition point (exceeding 0.7). Hence a long-range *repulsion* of micelles may be anticipated. That sort of interaction is considered in section 5.

Another useful piece of information comes from the AFM images (Figure 2): the area fraction of micelles is around $\phi \approx 0.9$ at 7 dyn/cm and $\approx$0.5 at 0.5 dyn/cm (with 20% accuracy). However, the areas per molecule are $A \approx 0.30$ and 0.33 nm^2, respectively. How come the ratio of ϕ's is 2 and that of the areas is 1.1? If the gaps between the micelles are surfactant free, then we arrive at the totally unreasonable conclusion that micelles at higher $P_s = 7$ dyn/cm are considerably *thinner* than at the lower P_s. It is therefore likely that the gaps between the micelles are not clean water but are covered by the surfactant. In other words the FnHm Langmuir layer is continuous (at least at $P_s \gtrsim 0.5$ dyn/cm), but its thickness is not constant: the film is thinner in the gaps (where the number density of molecules is $1/A_2$) and is thicker in the micelle regions (with higher number density $1/A_1$). This $A_1 - A_2$ model can easily rationalize the geometrical data. For example, assuming that the A_1 layer and A_2 layer are incompressible, we get the following lever rule for the mean area per molecule, A:

$$\frac{\phi}{A_1} + \frac{1-\phi}{A_2} = \frac{1}{A} \qquad (1)$$

Using the data quoted above we obtain

$$A_1 \approx 0.29\ \text{nm}^2, \quad A_2 \approx 0.39\ \text{nm}^2 \qquad (2)$$

The compressibility of the individual A_1 and A_2 layers may slightly affect the molecular areas, but the qualitative picture of the two surface phases with different densities stays intact.

The two-phase picture is further supported by the X-ray reflectivity and surface potential measurements on Langmuir layers of semifluorinated alkanes with slightly longer H-blocks (F8H18).[18,19] For molecular areas $A > 0.45$ nm^2, the reflectivity data[18] are consistent with a monolayer structure (the one-slab model[22]) of the Langmuir film of thickness $h = h_2 \approx 2.7$ nm. The electron density is nearly uniform (independent of the height)

(20) Bates, M. A.; Frenkel, D. *Phys. Rev. E* **2000**, *61*, 5223.
(21) Pronk, S.; Frenkel, D. *Phys. Rev. E* **2004**, *69*, art.no.066123.
(22) Born, M.; Wolf, E. *Principles of Optics*, 6th ed.; Pergamon Press: New York, 1991.

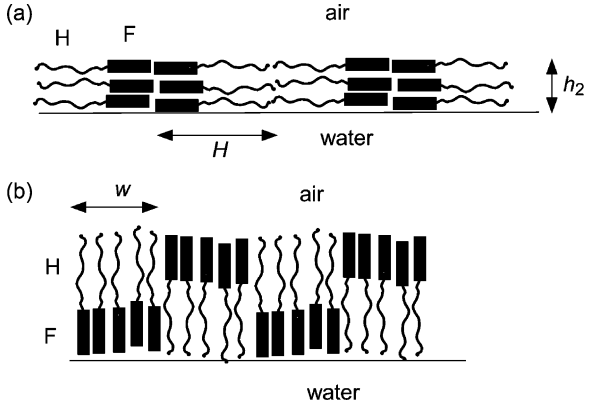

Figure 4. (a) Structure of the P-phase. (b) The FH/HF structure.

within the F8H18 surfactant layer.[18] What could be the structure of such uniform layer? A homogeneous distribution of F and H blocks is unlikely because these blocks are highly incompatible (the energy of transfer of one CH_2 group from an H to an F environment is about $0.5k_BT$). It must be expected that F and H fragments separate, forming a microdomain structure. Vertical separation is excluded as it would result in a strongly inhomogeneous height distribution of the electron density. Hence, a horizontal separation of F and H blocks is likely. The simplest structure of that sort is shown in Figure 4a: the FnHm molecules lay parallel to the surface; the F and H blocks form alternating stripes; each stripe is a bilayer of oppositely oriented similar blocks. This structure (which is referred to below as P phase) is obviously compatible with the observed vertically homogeneous electron density (the structure in the lateral direction is not probed by the X-ray reflectivity).

A different model was proposed in ref 18: a mixed FH/HF model, i.e., a domain structure with alternating vertically separated FH and HF (inverted) regions (Figure 4b). However, we believe that such a structure is hardly favorable, as discussed in Appendix C.

On the other hand, the reflectivity data obtained at $A \approx 0.30 \div 0.32$ nm^2 ($P_s \approx 4 \div 7$ dyn/cm) point to a vertically inhomogeneous FnHm layer structure for both F8H16 and F8H18 molecules (see refs 7, 8, 19). The calculated best fit layer thickness is $h_1 \approx 2.9$ nm for F8H16 and $h_1 \approx 3.3$ nm for F8H18. The two-slab FH-layer model was proposed in refs 7 and 8 for F8H16: the FnHm molecules are oriented nearly vertically with their hydrogenated segments directed toward water and their perfluorinated segments directed toward air (Figure 5a). A different structure (also with roughly vertical molecular orientation) was proposed for F8H18: a FH_2F bilayer involving three slabs in which the surfactant molecules are antiparallel with interpenetrating H blocks inside and F blocks outside[19] (see Figure 5b). It is natural to anticipate a 1st-order phase transition between the horizontal (P) structure of Figure 4a and a vertical structure of Figure 5. The FH_2F structure seems less realistic than the FH model since (i) fluorocarbons are more hydrophobic than hydrocarbons (F/water interfacial tension is higher than the tension at the H/water interface) and hence it is H-blocks that must be in contact with water (this conclusion is in accord with the results of X-ray diffraction and reflectivity studies on F12H18[9]; it was recently confirmed by X-ray reflectivity for Langmuir layers of F14H20[10]); (ii) the 3-slab model involves more fitting parameters, which may be the major reason for its slightly superior fit in ref 19; and (iii) in addition, one must bear in mind that the typical resolution in X-ray reflectivity studies is about 1 nm, hence the 3-slab model involving a sublayer thinner than 1 nm must be considered with caution. Therefore, we assume the FH structure

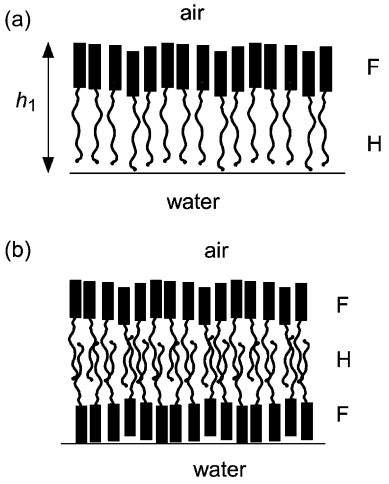

Figure 5. (a) Two-slab FH-layer structure of the vertical phase. (b) The three-slab FH_2F layer model.

for the high-density phase (see Figure 5a) in the rest of the paper: a two-slab layer of total thickness $h_1 \approx 3$ nm (with heights of the F and H sublayers of around $h_{1F} \approx 1.2$ nm and $h_{1H} \approx 1.8$ nm, respectively). [The thicknesses h_{1F} and h_{1H} are approximate with an error ± 0.2 nm; they correspond to the ratio of densities ρ_F and ρ_H in the F and H sublayers, $\rho_F/\rho_H \approx 2.7$. This ratio is a sort of a compromise between the typical ratio of the bulk densities of hydrocarbons and fluorocarbons, $\rho_F/\rho_H \approx 2.3$, and the ratios based on the thicknesses of F and H sublayers obtained from the reflectivity data on layers of F8H16 ($\rho_F/\rho_H \approx 3.4$, refs 7 and 8) and F8H18 molecules ($\rho_F/\rho_H \approx 2.7$, ref 23). ($\rho_F/\rho_H$) $\approx$ 2.70 can be also obtained using the ratio of electron densities in the F and H sublayers of F14H20 molecules as recently measured by X-ray reflectivity.[10]]

The two-phase scenario is also supported by the measurements of the surface electric potential U vs molecular area A for F8H18 layers. [The surface potential is due to the permanent dipole moment oriented roughly along the long axis of an FnHm molecule. The dipole moment consists of three contributions: localized at the CF_2-CH_2 bond, and near the ends of the F and H blocks.] They show[18] that U is nearly constant for both $A \lesssim 0.35$ nm^2 and $A \gtrsim 0.45$ nm^2, but U changes rapidly, in a linear fashion, in the range 0.35 nm^2 $< A <$ 0.45 nm^2. This behavior has been interpreted as a signature of a first-order phase transition between two different layer structures, with the phase separation region between $A_1 \approx 0.33$ nm^2 and $A_2 \approx 0.45$ nm^2.

4. Two Main Structures of the FnHm Layers

4.1. Vertical Phase. The structure of the vertical (FH) phase is shown in Figure 5a. It consists of an F sublayer in contact with air and an H sublayer in contact with water, with a thin electrically polarized interface between the F and H sublayers. The dipole moment of the layer is oriented downward, possibly at some angle with the normal to the layer. The dipole moment is mainly localized near the interface between F and H sublayers with positive H and negative F units. The surface potential $U = 4\pi\sigma$, where $\sigma = \mu_\perp/\epsilon A$, $\mu_\perp$ is the vertical component of the dipole moment per molecule, A is the area per molecule, and ϵ is the effective dielectric constant. The surface potential measured in the vertical phase of F8H18 is $U \approx 0.9$ V;[18] we will use this value in what follows. [A similar surface potential was obtained for

(23) El Abed, A.; Ionov, R.; Daoud, M.; Abillon, O. *Phys. Rev. E* **2004**, *70*, 051607.

F10H14.[24] The lower $U \approx 0.6$ V obtained for F8H16[24] is probably characteristic of a microdomain phase (see below, section 5.3) where a fraction $(1 - \phi)$ of the area is occupied by nonpolar domains that does not contribute to U. In addition, nonequilibrium effects must be stronger in the study[24] due to the higher (standard) compression speed as compared to the reduced speed of the compressing barrier used in ref 18.] Therefore

$$\sigma = \frac{U}{4\pi} \approx 2.4 \times 10^{-4}\ \text{CGS} \tag{3}$$

The free energy per unit area of the layer is

$$F = F_\gamma + F_{\text{conf}}, \quad F_\gamma = \gamma_{\text{Hw}} + \gamma_{\text{Fa}} + \gamma_{\text{FH}} - \gamma_{\text{w}} \tag{4}$$

where $\gamma_{\text{w}} \approx 70$ dyn/cm is the surface tension of water and γ_{Hw}, γ_{Fa}, and γ_{FH} are the surface tensions at the interfaces between hydrogenated blocks and water, fluorinated blocks and air, and fluorinated and hydrogenated blocks, respectively. We estimate γ_{Fa} as the surface tension of Teflon at 20 °C, $\gamma_{\text{Fa}} \approx 20$ dyn/cm;[25] γ_{Hw} is estimated based on the surface tension of polyethylene ($\approx$31 dyn/cm[25]) and the contact angle of a water droplet on the PE surface ($\approx 90°$ [26]): $\gamma_{\text{Hw}} \approx 30$ dyn/cm. The energy of the FH interface is not known; we expect that it is significant ($\gamma_{\text{FH}} >$ 20 dyn/cm): it incorporates a contribution of local (van der Waals) interactions of incompatible CF_2 and CH_2 units and also the electrostatic energy of the dipole layer. It is therefore likely that $F_\gamma > 0$. The positive F_γ is the driving force for the self-assembly of the FnHm molecules in a Langmuir layer. The layer tends to become thicker because of positive F_γ; this tendency is opposed by an increase of the conformation energy F_{conf}. So, the layer thickening stops when F blocks become extended in the vertical direction. The resultant thickness at the area per molecule $A = A_1 \approx 0.29$ nm^2 is $h = h_1 \approx 3$ nm.

4.2. P Phase. The tentative structure of the parallel (P) phase is shown in Figure 4a: an FnHm layer of thickness $h = h_2$ consisting of stripes in the lateral direction. Each F (H) stripe is a bilayer of antiparallel F (H) blocks. Each FnHm molecule spans a half of an F domain and a half of an H domain; that is, the structure can also be viewed as a sequence of alternating FH and HF molecular sublayers. Statistically, an FH sublayer is a mirror reflection of the next HF sublayer; two sublayers (FH and HF) constitute a period. We *assume* that the molecular packing in an FH sublayer is the same as in the vertically separated FH phase (expected at $A = A_1$). Thus, the volume per molecule in both phases (parallel and vertical) must be the same, i.e., $h_2 = h_1A_1/A_2 \approx 2.2$ nm (this thickness can be compared with the experimental $h_2 \approx 2.7$ nm for F8H18[18]). Further, the half-period of the lateral structure is $H = h_1 \approx 3$ nm, and the surface potential U at each FH interface is roughly $U \approx 0.9$ V. According to the thicknesses of F and H sublayers in the vertical phase mentioned in section 3, the half-width of an F stripe is $H_{\text{F}} \approx 1.2$ nm, and that of an H stripe is $H_{\text{H}} \approx 1.8$ nm; that is, the area fraction of F domains is $f_{\text{F}} \approx 0.4$. The free energy of the layer can be written as

$$\mathcal{F} = \gamma^* \mathcal{A} + \mathcal{F}_{\text{FH}} + \text{const} \tag{5}$$

where $\mathcal{A}$ is the total area of the layer

$$\gamma^* = (\gamma_{\text{Fa}} + \gamma_{\text{Fw}})f_{\text{F}} + (\gamma_{\text{Ha}} + \gamma_{\text{Hw}})(1 - f_{\text{F}}) - \gamma_{\text{w}} \tag{6}$$

is the energy of interfaces with water and air (i.e., the surface energy variation on replacing the water/air interface by the water/FnHm and FnHm/air interfaces), $\mathcal{F}_{\text{FH}}$ is the energy of interfaces between F and H domains, and const incorporates the FnHm conformation free energy which is nearly independent of the thickness $h = h_2$. Here γ_{Fw} is the tension at the interface between the F domain and water, γ_{Ha} is the tension at the upper surface of H stripes; the other γ's are defined in the previous subsection. The FH interfacial energy is

$$\mathcal{F}_{\text{FH}} = \gamma_{\text{FH}} h\mathcal{A}/H + \mathcal{F}_{\text{e}} \tag{7}$$

where γ_{FH} (introduced in the previous subsection) is the surface energy per unit area of an infinite FH interface, $h\mathcal{A}/H$ is the total area of FH interfaces, and $\mathcal{F}_{\text{e}}$ accounts for the edge effects which are mainly due to the electrostatic interactions of dipole layers.

To determine the electrostatic edge energy $\mathcal{F}_{\text{e}}$, we model the system as a sequence of thin dipole layers with uniform density of dipole moment ($\sigma \equiv \mu_\perp/(A\epsilon) = U/(4\pi)$ for odd and $-\sigma$ for even layers). Each dipole layer is of height h, of width $w \ll h$, and of infinite length. We assume that the FnHm layer is dielectrically uniform, with a dielectric constant intermediate between $\epsilon \approx 2.1 \div 2.4$ typical of polyethylene and $\epsilon \approx 2$ for Teflon.[27] Thus, the dielectric constant is $\epsilon = \epsilon_{\text{w}} \approx 80$ (water) for $z < 0$, $\epsilon \approx 1$ for $z > h$ (air), and $\epsilon = \epsilon_1 \approx 2.2$ for $0 < z < h$ (the FnHm layer). Further, we neglect $1/\epsilon_{\text{w}}$, i.e., set $\epsilon_{\text{w}} = \infty$. Benefiting from the mirror-image principle and calculating the electrostatic energy in the logarithmic approximation (for $H > h \gg w$), we get

$$\mathcal{F}_e \simeq -C\mathcal{A} \ln \frac{h}{w}, \quad C = 2\epsilon_1 \frac{2 + \epsilon_1}{1 + \epsilon_1} \sigma^2/H \tag{8}$$

On using eqs 5, 7, and 8, the total energy becomes

$$\mathcal{F} = \mathcal{V}\left(\frac{\gamma^*}{h} + \frac{\gamma_{\text{FH}}}{H} - \frac{C}{h} \ln \frac{h}{w}\right) \tag{9}$$

where $\mathcal{V} = h\mathcal{A}$ is the total layer volume which is kept nearly constant (independent of h) due to the low volume compressibility of the layer. If $\gamma^* < 0$, then $\mathcal{F}$ is decreasing as h is decreased (in the region $h \gg w$ where eq 8 is valid), so that the FnHm layer tends to cover the whole available water surface. The surface pressure in this case is positive and does not vanish, even at high $\mathcal{A}$'s. This is in contrast with the surface pressure measurements[7,8,18] indicating that P_{s} strongly decreases with $\mathcal{A}$ and is almost 0 for $\mathcal{A} \gtrsim 0.45$ nm^2. Therefore $\gamma^* > 0$. Minimizing the total energy $\mathcal{F}$ with respect to h, with the side condition $h\mathcal{A} =$ const, we get

$$h \sim we^{1+\gamma^*/C} \tag{10}$$

where $C = 2\epsilon_1[(2+\epsilon_1)/(1+\epsilon_1)](\sigma^2/H) \approx 1$ dyn/cm. The width w can be roughly estimated as $w \sim 0.3$ nm (twice the C−C bond length). The anticipated height $h = h_2 \approx 2.2$ nm (see the beginning of this section) is compatible with eq 10 if $\gamma^*/C \sim 1$, i.e., $\gamma^* \sim 1$ dyn/cm. To summarize, the above model shows that the P phase of reasonable finite thickness can be stable if γ^* is positive and low. This is possible since γ^* is defined as a *difference* of surface tensions. However, this requirement implies a subtle balance between the tensions involved in eq 6: both $\gamma_{\text{Fa}} + \gamma_{\text{Fw}}$ and $\gamma_{\text{Ha}} + \gamma_{\text{Hw}}$ must be close to the water surface tension γ_{w}.

4.3. Coexistence of FH and P Phases. As explained in sections 3 and 4, the FnHm Langmuir film is separated into two phases

(24) Broniatowski, M.; Minones, J., Jr.; Sandez Macho, I.; Dynarowicz-Latka, P. *Pol. J. Chem.* **2005**, *79*, 1047.
(25) http://www.gewater.com/library/tp/772_Hydrophilicity_ and.jsp
(26) Kim, M. S.; et al. *Polym. Prepr.* **2005**, *46*, 166.
(27) *CRC Handbook of Tables for Applied Engineering Science*; CRC Press: Boca Raton, FL, 1973.

(FH phase with roughly vertical and P phase with roughly horizontal orientations of molecules) if the molecular area $A < A_2$. The transition area $A_2 \approx 0.39$ nm^2 for F8H16 (see eq 2). The area A_2 can be estimated for different FnHm molecules based on the surface potential measurements (interpreting A_2 as the surface area corresponding to the onset of a strong variation of the surface potential): $A_2 \approx 0.53$ nm^2 for F8H16 and F8H17,[24,28] $A_2 \approx 0.45$ nm^2 for F8H18,[18] and $A_2 \approx 0.35$ nm^2 for F6H18.[24] It is remarkable that the surface pressure P_s measured at $A = A_2$ was zero in all of the cases within the experimental error (which was typically ± 0.1 dyn/cm). According to the classical phase separation scenario this result must mean that the two phases, FH and P, are always at coexistence at $P_s = 0$, i.e., that the free energies of the two phases are equal at $P_s = 0$ for various FnHm molecules. On the other hand, this conclusion is highly unprobable since, based on the general grounds, one must anticipate that the difference of free energies of FH and P phases must depend on the block lengths n and m (note that the typical free energy per unit area is around 10 dyn/cm, i.e., 100 times higher than the experimental inaccuracy). It seems that the only way out of this contradiction is to assume that the surface pressure at the phase coexistence, P_{12}, is actually negative ($P_{12} < 0$) for most of the FnHm molecular structures (including probably F8H16). In other words, we tend to assume that the less dense P phase is actually metastable (since a negative pressure is not possible at a genuine equilibrium). The following sequence of transformations of the FnHm layer is anticipated in this case at high areas per molecule A (at $P_s \simeq 0$).

(1) Initially, the FnHm molecules are more or less randomly distributed on the surface (we can talk about "surface gas" of these molecules).

(2) Then the molecules spontaneously condense forming small islands of P phase surrounded by very dilute surface gas phase.

(3) As the P islands grow, the more favorable FH phase nucleates in them, so P islands turn to FH islands once the island diameter exceeds a certain threshold $D = D^*$. The size D^* can be defined in the following way: We assume that the edge tension of the FH phase is higher than that of the P phase: $\lambda_{FH} > \lambda_P$ (in particular, because the FH phase is thicker). A small island prefers to be in the P-state since its edge energy is lower in this state. The equilibrium transition takes place when the difference between the free energies of the two states vanishes: $\mathcal{F}_{FH} - \mathcal{F}_P = 0$. This difference can be approximately written as

$$\mathcal{F}_{FH} - \mathcal{F}_P \approx \pi D(\sqrt{A_1/A_2}\lambda_{FH} - \lambda_P) + \frac{\pi}{4} D^2\left(\frac{A_1}{A_2} f_{FH} - f_P\right)$$

where f_{FH} and f_P are the free energies per unit area at $P_s = 0$ in the infinite P and FH layers, respectively (A_1/A_2 is the ratio of the island area in the FH state to that in the P state). Note that $(f_{FH} + P_{12})A_1 = (f_P + P_{12})A_2$ and $P_{12} < 0$. Therefore, $D^* \approx 4(\sqrt{A_1/A_2}\ \lambda_{FH} - \lambda_P)/[|P_{12}|(1 - A_1/A_2)]$. It is not currently possible to estimate D^* using this relation as the edge energies λ_{FH} and λ_P are not known with sufficient precision.

(4) The FH islands grow further. There are two principal mechanisms of this growth: diffusion-coalescence (Lifshitz–Slyozov mechanism of Ostwald ripening) and collision-coalescence (fusion). The rate of diffusion coalescence is proportional to the 2-dimensional concentration in the "surface gas" phase which is extremely dilute. The first mechanism is therefore suppressed; that is, the growth is mainly due to the fusion of islands (see Appendix A). The growth of islands is therefore limited due to their electrostatic repulsion (see the next section).

(5) As A decreases below a certain threshold ($A < A_m$), the surface gas-phase disappears; at this stage, a continuous Langmuir layer is formed. The structure of this layer is analyzed in the next section.

5. Surface Micelle Formation

5.1. Dipole–Dipole Interaction Energy. The FH islands repel each other due to electrostatic interaction of dipole layers localized at the F/H interfaces.

Let us derive the general expression for the energy of dipole–dipole interactions $\mathcal{F}_e$. We can take advantage of a few simplifications. First, since $\mathcal{F}_e$ comes from the long-range effects (with lateral length-scale $\gg 1$ nm), the distribution of dipoles across the FnHm layer is irrelevant. It is convenient to divide the layer into cells of size ξ, $D \gg \xi \gg h$. Then $\mathcal{F}_e = \sum_{i<j} \mathcal{F}_{ij}$, where $\mathcal{F}_{ij}$ is the energy of interaction of cells i and j which is proportional to the cell dipole moments m_i and m_j. The system is dielectrically inhomogeneous: the dielectric constant $\epsilon = \epsilon_w \approx 80$ in water, i.e., for $z < 0$ ($z = 0$ defines the water/film interface), and $\epsilon \approx 1$ in air ($z > h$). It is convenient to define m_i as the genuine total dipole moment of cell i, including both "permanent" and "induced" dipoles, instead of considering the FnHm layer as a dielectric medium. Then, we must formally set $\epsilon = 1$ in the FnHm layer since all of the polarization effects are included in the definition of the cell moment. Note that thus defined m_i is directly proportional to the surface potential U of the cell: $m_i = \sigma \mathcal{A}_i$, where $\mathcal{A}_i$ is the cell area. [Note that m_i is the vertical projection of the dipole moment: its horizontal component is not relevant.] Further, we treat $1/\epsilon_w$ as a small parameter, and use the mirror-image principle, neglecting corrections of the order $1/\epsilon_w$. The electric field induced by the dipole m_i at the cell j, E_{ij}, is therefore nearly twice the electric field induced by that dipole in the vacuum: $\underline{E}_{ij} \simeq -2(m_i/r^3)\underline{e}_z$, where r is the distance between the cells i and j, and e_z is the unit vector along the vertical z axis. [Note that E_{ij} is the genuine electric field induced by the dipole m_i (and by its mirror image in the water surface) at the cell j; there are no additional contributions due to "induced" dipoles since all the polarization effects are already included in the definition of the cell dipole moments.] A variation δm_j of the second dipole moment results in the energy variation $\delta \mathcal{F}_{ij} = -\underline{E}_{ij} \cdot \underline{e}_z\, \delta m_j$. Thus, we get

$$\mathcal{F}_e \simeq \int \frac{\sigma(r_1)\sigma(r_2)}{r_{12}^3} d^2r_1 d^2r_2 \qquad (11)$$

where r_{12} is the distance between r_1 and r_2, $r_{12} > r_{min}$, r_{min} is the short-scale cutoff, d^2r is the area element, and $\sigma(r)$ is the local dipole moment per unit area: $\sigma(r) = \sigma_0$ in the islands of FH phase and $\sigma(r) = 0$ in the "surface gas" or P phase outside. (The mean dipole moment in the P phase is zero since the dipole moments of neighboring FH interfaces between the stripes compensate each other, and a similar compensation comes from the mirror image of the horizontal dipoles in the water surface.)

Equation 11 can be transformed as (an unimportant local short-range electrostatic contribution is omitted from $\mathcal{F}_e$)

$$\mathcal{F}_e \simeq -\int \frac{\nabla\sigma(r_1)\cdot\nabla\sigma(r_2)}{r_{12}} d^2r_1 d^2r_2 = -\sigma_0^2 \int \frac{d\underline{s}_1 \cdot d\underline{s}_2}{r_{12}} \qquad (12)$$

where $d\underline{s}$ is the properly oriented displacement vector element

(28) Broniatowski, M.; Sandez Macho, I.; Minones, J., Jr.; Dynarowicz-Latka, P. *Appl. Surf. Sci.* **2005**, *246*, 342.

along the edge and σ_0 is defined in eq 3. The region of integration in eq 12 is restricted by the condition $r_{12} > r_{min}$ (thereby we get rid of the short-range contributions to $\mathcal{F}_e$). We set $r_{min} = 1$ nm; a precise value of r_{min} is not really important: a change of r_{min}, say, from 1 to 2 nm is equivalent to just a small renormalization of the edge line tension: $\lambda \to \lambda - 2\sigma_0^2 \ln 2$.

5.2. Interaction of Two FH Islands. Let us consider first the electrostatic interaction of two FH islands (both of diameter D, the distance between their centers is L). The interaction energy F_{int} can be defined, using eq 12, as $F_{int} = \mathcal{F}_e(2 \text{ islands}) - 2\mathcal{F}_e(1 \text{ island})$. Whence

$$F_{int} \simeq -2\sigma_0^2 \int \frac{d\underline{s}_1 \cdot d\underline{s}_2}{r_{12}} \tag{13}$$

where $d\underline{s}_1$ and $d\underline{s}_2$ are the perimeter elements of the first and the second island, respectively, and the factor 2 reflects the equivalent contribution due to the interchange of the regions of $d\underline{s}_1$ and $d\underline{s}_2$ integrations. Thus we get

$$F_{int} = F_{int}(L, D) = \sigma^2 D I(x) \tag{14}$$

where $x = L/D$

$$I(x) = 4 \int_{-\pi/2}^{\pi/2} d\alpha \int_0^{\pi/2} d\beta \frac{\cos 2\beta}{(x^2 + 2x \sin\alpha \cos\beta + \cos^2\beta)^{1/2}} \tag{15}$$

Note that $I(1) = (8/\pi)\Gamma(3/4)^4 \approx 5.74$; $I(x) \simeq I(1) - 4\pi[2(x - 1)]^{1/2}$ for $x - 1 \ll 1$; for large $x \gtrsim 1.5$, the reduced interaction energy $I(x)$ rapidly vanishes as $I(x) \simeq \pi^2/(8x^3)$. Two islands cannot fuse unless they touch each other. The corresponding state, when the islands just touch each other, is the activation state for their fusion. The activation energy U is due to their electrostatic repulsion: $U \approx F_{int}(D, D) - F_{int}(\bar{L}, D)$, where $\bar{L} \approx D/\sqrt{\phi}$ is the typical distance between the islands. Using eqs 14 and 15, we get for $\phi \lesssim 1/2$

$$U \approx 5\sigma^2 D$$

the fusion time τ therefore is

$$\tau \sim \tau_0 e^{U/k_B T}$$

where $\tau_0 \sim 6\pi\eta(D/2)^3/k_B T$ is the time of free diffusion of an island on the distance $\sim D/2$ (see Appendix A). The experimental time ranges from ~10 min (surface pressure measurements) to several hours (X-ray). Using the equations above, we find that $\tau = 5$ min corresponds to $D \approx 24$ nm, $\tau = 10$ h, to $D \approx 32$ nm. The range of $D^* = 24 \div 32$ nm nearly coincides with the range of sizes of the observed surface micelles. It is therefore likely that the micelles are islands of the FH phase that do not grow further because of the electrostatic repulsion. Accordingly, the FH islands are referred to as "micelles" in the rest of the paper.

5.3. Aggregation of FH Islands at $P_s \simeq 0$. Large enough FH islands (of size D^* or larger) do not fuse as explained in the previous section. However, they can aggregate according to the following mechanism: (1) Two neighboring FH islands (micelles) of size D come close to each other, so that the distance between their edges is D' and (2) then a small P island of size D' forms a bridge between the micelles (see Figure 6a). The electrostatic energy penalty, ΔF_e, emerged at the first stage can be easily compensated by the edge energy gain, ΔF_{edge}, due to a replacement of parts of FH and P edges by the FH/P interface at the second stage. For example, consider $D = 24$ nm, $D' = D/4$. Then ΔF_{int}

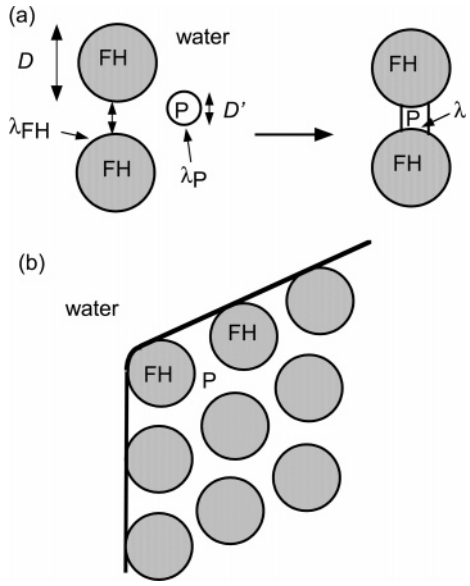

Figure 6. (a) Formation of a P bridge between FH islands (the edge tensions are indicated by arrows); "water" means clean water surface (the "surface gas" phase). (b) A fragment of the microdomain FH/P phase. The surfactant/water boundary is shown by the thick line.

$= F_{int}(D + D', D) - F_{int}(\bar{L}, D) \sim 3k_B T$, $\Delta F_{edge} \approx -(D/2)[0.5\lambda_P + 0.77(\lambda_{FH} - \lambda)] \approx -0.64\lambda_P D$, where in the last equation we assumed that $\lambda_{FH} - \lambda \approx \lambda_P$ (λ is the line tension at the FH/P interface). Thus, the bridge formation is favorable, $\Delta F = \Delta F_{int} + \Delta F_{edge} < 0$ if

$$\lambda_P \gtrsim 0.8 \times 10^{-7} \text{ dyne} \tag{16}$$

The edge tension λ_P at the P phase/water interface is expected to be similar to λ_{FH}: $\lambda_P \sim \lambda_{FH} \sim 10^{-6}$ dyne (see Appendix A). The above condition (16) is therefore likely to be valid. Hence, aggregation of FH micelles must be favorable and straightforward (it is not hindered by any considerable activation energy barrier). In a large aggregate, the P bridges tend to merge and to form a continuous P matrix (thereby reducing the energy of surfactant/water line boundaries). A continuous microdomain surface phase is formed as a result (see Figure 6b).

The microdomain FH/P phase can be formed even if small P islands are not available. In this case the P bridges, and eventually the P matrix, are formed by transforming certain (thin) peripheral regions of FH islands into the P phase state. Let us check the thermodynamic stability of the microdomain phase at $P_s \simeq 0$ by comparing its free energy with the free energy of isolated FH micelles.

The free energy of one isolated disklike FH micelle of size D_0 is

$$F_0 = f_{FH} A_0 + \pi\lambda_{FH} D_0 + F_e(D_0) \tag{17}$$

where f_{FH} is the free energy per unit area in an infinite FH layer, $A_0 = \pi D_0^2/4$ is the micelle area, the second term in the rhs is the micelle edge energy, and the last term F_e is the long-range electrostatic correction to the edge energy. It is assumed that D_0 is much larger than the FH-layer thickness, $D_0 \gg h_1$. The electrostatic energy is calculated in the logarithmic approximation using eq 12. The result reads

$$F_e(D_0) \simeq -2\pi\sigma^2 D_0 \left(\ln \frac{2D_0}{r_{min}} - 2\right) \tag{18}$$

The free energy of the condensed microdomain phase (see Figure 6b) per micelle is

$$F = f_{FH}A' + f_PA'' + \pi\lambda D + F_e(D) + 3F_{int}(L, D) \quad (19)$$

Here $A' = \pi D^2/4$ is the area of one FH domain, πD is its perimeter, A'' is the area of P matrix per micelle, λ is the FH/P edge tension, and L is the distance between the centers of neighboring FH domains. The edge line tension λ incorporates the effects of local van der Waals and electrostatic interactions (with length scales $\lesssim r_{min}$). The edge energy is due to the deformations of the unfavorable interfaces and due to conformational distortions of FnHm molecules at the boundaries between the FH and P phases. The last term, $3F_{int}$, in eq 19 is the energy of electrostatic interactions of micelles; F_{int} is defined in eq 14 and the factor $3 = 6/2$ comes from 6 nearest neighbors (interactions of nonnearest neighbors are much weaker and are neglected).

The interaction energy is calculated assuming that FH domains (micelles) are arranged in a hexagonal lattice (with lattice parameter L), which is true (at least) at high enough surface pressure $P_s \gtrsim 0.5$ dyn/cm. At lower P_s (in particular, at $P_s = 0$), the micelles may not be ordered. However, in this regime, the interaction energy must be small (amounting to $\lesssim k_BT$ per micelle), so this energy is negligible in comparison with other energy terms (for example, the edge energy $\pi\lambda D$, which is typically $\gtrsim 50k_BT$). (For the same reason, the translational ideal-gas free energy accounting for fluctuations of micelle positions is also negligible.) Thus, the "hexagonal" approximation works at any P_s.

Obviously

$$A' + A'' = \sqrt{3}L^2/2 \equiv A_{cell} \quad (20)$$

(A_{cell} = the hexagonal cell area). The total number of molecules in a cell coincides with that in an original isolated micelle since micelles do not appear/disappear during the aggregation process

$$A'/A_1 + A''/A_2 = A_0/A_1 \quad (21)$$

where A_1 and A_2 are defined in eq 2. The thermodynamic equilibrium of FH and P phases at $P_s = P_{12}$ demands that the corresponding chemical potentials are equal

$$(f_{FH} + P_{12})A_1 = (f_P + P_{12})A_2 \quad (22)$$

(here we neglect the compressibility of both phases at low P_s). Using eqs 21 and 22, we find

$$f_{FH}A' + f_PA'' - f_{FH}A_0 = -P_{12}A''(1 - A_1/A_2)$$

The free energy of the condensed phase can be obtained by minimization of F, eq 19, with respect to D (with conditions, eqs 20 and 21). The difference $F - F_0$ depends on λ, λ_{FH}, and D_0. It must be anticipated that $\lambda < \lambda_{FH}$: the boundary between FH phase and clean water costs more energy than the boundary between FH and P surfactant phases. Then we find that the condensed phase is thermodynamically more stable than isolated FH micelles, $F < F_0$, even if $P_{12} < 0$, provided that $|P_{12}|$ is not too high. For the typical edge tensions $\lambda_{FH} \sim 10^{-6}$ dyne, $\lambda \sim 3 \times 10^{-7}$ dyne (note that the value $\lambda = 2.6 \times 10^{-7}$ dyne is considered in the next section) and $D_0 \sim 30$ nm, we find that the condensed phase is favorable if $|P_{12}| < 20$ dyn/cm. The latter condition is likely to be true: $|P_{12}| \lesssim 1$ dyn/cm for F8H16 molecules (see the next section).

5.4. Surface Pressure vs Molecular Area. A compression of the microdomain phase results in an increase of surface pressure P_s which can be calculated using eqs 19−22

$$P_s = -\frac{\partial F}{\partial A_{cell}} \quad (23)$$

where the derivative is taken at constant number of molecules (i.e., A_0 = const, see eq 21). Note that the number of micelles does not change since their fusion is suppressed by electrostatic repulsion; the micelle "evaporation" process (implied in the Lifshitz−Slyozov coalescence mechanism of Ostwald ripening) is also suppressed by the effect discussed in section 6. Note also that the dependence of P_s on P_{12} is trivial

$$P_s = \text{const} + P_{12} \quad (24)$$

at any given set of parameters A_0, A, and λ.

There are two unknown parameters, λ and P_{12}, involved in eq 19 (the additional parameter A_0 involved in eq 21 is set by the condition: $D \approx 26$ nm at $P_s \approx 0.5$ dyn/cm in accordance with the AFM data). One may wonder if it is possible to find these parameters by fitting the theoretical dependence, P_s vs A, to the experimental data. This does not really work since the dependence of P_s on both parameters is relatively weak, as compared to the uncertainty of the experimental data (most importantly, of the parameter A_2 calculated using the data). What can be reliably concluded is that $\lambda < 10^{-6}$ dyne and $|P_{12}| < 1$ dyn/cm. To get a better estimate for λ and P_{12}, we invoke an additional information: the AFM and GISAXS data (refs 7, 8, and 12 and Figures 2 and 3) suggest that micelles are less polydisperse and are better ordered in a hexagonal structure at $P_s \approx 0.5$ dyn/cm than at $P_s \approx 0$. It is therefore reasonable to assume that the pressure threshold for the interaction-driven suppression of micelle polydispersity is $P^* \lesssim 0.5$ dyn/cm (see section 6). Setting $P^* = 0.5$ dyn/cm and fitting the calculated $P_s(A)$ dependence, we get $\lambda \approx 2.6 \times 10^{-7}$ dyne, $P_{12} \approx -0.25$ dyn/cm (see Figure 7). These values must still be considered as just rough estimates. The agreement between the predicted P_s and the experimental is quite reasonable given the approximations and experimental errors involved. Some deviation between the experimental and the theoretical curve at high compressions can be attributed to a finite compressibility of the FH and P sub-phases which is not allowed for in the theory (as a result the theoretical P_s diverges as $A \to 0.297$ nm^2, i.e., as $\phi \to \phi_{max}$, where $\phi_{max} = \pi/2\sqrt{3} \approx 0.91$ is the area fraction of closely packed circles).

Note that the theoretical $P_s = 0$ for $A > A_m$, $A_m \approx 0.34$ nm^2. In this regime, the surface system separates macroscopically forming two phases: the microdomain FH/P phase and dilute phase (clean water with few surfactant islands). Signs of this macroscopic separation are clearly visible in the AFM image, Figure 3, obtained at $P_s \approx 0$, $A \approx 0.41$ nm^2.

5.5. Crystallization of Micelles. Let us turn to the transition from liquid of micelles to their ordered hexagonal array (2-dimensional micellar crystal). The question is: provided that the micelles are sufficiently monodisperse, at which molecular area A is this transition expected? The relevant essential parameter is the osmotic surface pressure of micelles, $\Pi = -(\partial\mathcal{F}/\partial\mathcal{A})|_{\mathcal{A}_{tot}=\text{const}}$ ($\mathcal{F}$ is the total free energy of the condensed surface phase, $\mathcal{A}_{tot}$ is its total area, and $\mathcal{A}$ is the area of the region where FH micelles are located; $\mathcal{A}$ is decreased keeping the number of micelles constant). In fact, the transition takes place when the hexagonal lattice is destabilized by numerous enough defects. The energy of a defect (for example, a vacancy) formation is essentially proportional to the osmotic pressure Π times the excess area associated with the defect. (The total surface pressure P_s is not directly relevant since micelle rearrangements can occur at a constant total area of the condensed phase.) Using the nearest-neighbor approximation (in analogy with eq 19), we get

$$\Pi \approx -\frac{\sqrt{3}}{L}\frac{\partial F_{\text{int}}}{\partial L} = -\frac{\sqrt{3}}{L}\sigma^2\frac{\mathrm{d}I(x)}{\mathrm{d}x}$$

where $x = L/D$. Computer simulations of 2-dimensional systems of hard disks indicate that the transition from the liquid state to hexagonal crystal occurs at $\Pi \approx 9(k_BT/D^2)$.[20] Applying this criterion and using the micelle parameters considered above, we get: $\tilde{\Pi} \equiv (\Pi D^2/k_BT) \approx -(\sqrt{3}\sigma^2 D/k_BTx)(\mathrm{d}I(x)/\mathrm{d}x)$, so the transition ($\tilde{\Pi} \approx 9$) occurs at $A = A_c \approx 0.33\ \text{nm}^2$. The experimental surface pressure at this point is $P_s = P^c \approx 0.5$ dyn/cm (the theoretical surface pressure at this point is ≈0.1 dyn/cm). This prediction is in agreement with the experimental ordering threshold of ≲0.5 dyn/cm (see section 3). Note that in view of eq 24 the critical pressure is $P^c = P^c{}_0 + P_{12}$, where $P_0{}^c$ depends on σ^2 and λ, but it does not depend on P_{12}.

It is important to recall that so far it has been assumed that the micelles are monodisperse. As we show in the next section, this assumption is likely to be valid for $P > P^*$, where the threshold P^* depends on γ and other parameters. The regime where micelles are arranged in a hexagonal lattice is therefore ultimately defined by the condition $P > \max(P^c, P^*) = \max(P_0{}^c, P_0{}^*) + P_{12}$ ($P_0{}^*$ is defined at the end of the next section).

6. Interaction Driven Suppression of Micelle Polydispersity

In the previous section, we assumed that the micelles are monodisperse at high surface pressures. This assumption is discussed below. First, we stress that well-separated (noninteracting) micelles are intrinsically polydisperse: larger micelles grow at the expense of smaller ones as long as the typical micelle size is much smaller than the equilibrium size. The situation changes at higher micelle concentration: interactions between micelles may render unfavorable an increase of one micelle accompanied by a decrease of another one.

To check this qualitative idea, we calculate the total free energy increment associated with an arbitrary small variation of micelle sizes. The reference state is a perfect hexagonal crystal of monodisperse micelles. An arbitrary (but small) distortion of the hexagonal lattice (perhaps induced by the micelle size variations) is also allowed.

The free energy of the system (with the prescribed total area of the film $\mathcal{A}$ and total area of the FH micelles $\mathcal{A}_m$) is

$$\mathcal{F} = \mathcal{F}_0 + \mathcal{F}_{\text{int}}$$

where $\mathcal{F}_0$ is the total self-energy (essentially, the edge energy) of the micelles, and $\mathcal{F}_{\text{int}}$ is the energy of their interactions. [Translational (ideal-gas) free energy of micelles is neglected here since it is dominated by the interaction and the edge energy terms: their typical magnitude is $\gg k_BT$ per micelle.]

$$\mathcal{F}_0 = \sum_{\underline{a}} F_0(D_{\underline{a}})$$

where $\underline{a}$ is the unperturbed position vector of a micelle center, $\underline{a}$ takes all possible values on the hexagonal lattice, $D_{\underline{a}}$ is the diameter of the micelle $\underline{a}$, $F_0(D_{\underline{a}})$ is its self-energy, i.e., the free energy of an isolated micelle of diameter $D_{\underline{a}}$ defined in eq 17 (where D_0 must be replaced by $D_{\underline{a}}$). With $D_{\underline{a}} = D^{(0)} + d_{\underline{a}}$ and

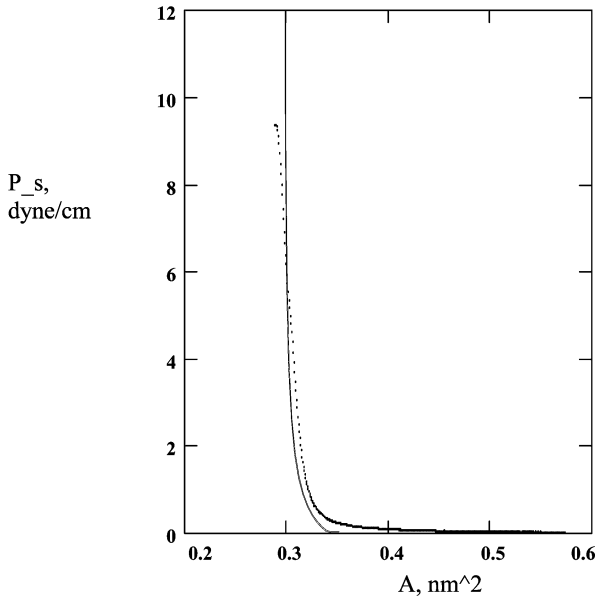

Figure 7. Dependence of surface pressure P_s on molecular area A for F8H16: the theory (solid line) and the experimental data (dots).[7,8]

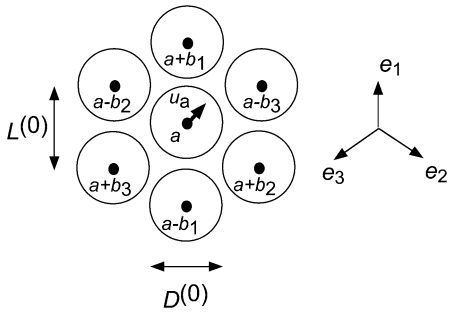

Figure 8. Micelle a and its 6 neighbors in the hexagonal structure.

with small $|d| \ll D$ the self-energy is

$$\mathcal{F}_0 \simeq \text{const} + \pi\lambda'\sum_a d_a + \frac{1}{2}\pi\lambda''\sum_a d_a{}^2 = \text{const} - \frac{\pi\tilde{\lambda}}{2D^{(0)}}\sum_a d_a{}^2$$

where $\lambda' = (1/\pi)\partial F_0(D)/\partial D$, $\lambda'' = \partial\lambda'/\partial D$, and the second equation comes from the micelle area conservation

$$\sum_a D_a{}^2 = \text{const} \qquad (25)$$

Here $\tilde{\lambda} = \lambda' - \lambda''D^{(0)} \simeq \lambda - 2\sigma^2(\ln(2D/r_{\min}) - 2)$ is the effective edge tension.

The interaction energy is

$$\mathcal{F}_{\text{int}} = \sum_a\sum_b F_{\text{int}}(L_{a,b}, D_a, D_{a+b})$$

where the vector $\underline{b}$ takes 3 values ($\underline{b}_1 = L^{(0)}\underline{e}_1$, $\underline{b}_2 = L^{(0)}\underline{e}_2$, and $\underline{b}_3 = L^{(0)}\underline{e}_3$) corresponding to the "bonds" between neighboring micelles (see Figure 8; the unit vectors $\underline{e}_1$, $\underline{e}_2$, and $\underline{e}_3$ form a perfect triangle), $L_{a,b}$ is the actual distance between the centers of micelles $\underline{a}$ and $\underline{a} + \underline{b}$ after the deformation, $F_{\text{int}}(L, D_1, D_2)$ is the interaction energy of two micelles of diameters D_1 and D_2 with their centers at the distance L, and F_{int} is defined in eq 13. The lattice deformation corresponding to displacements of micelle centers from $\underline{a}$ to $\underline{a} + \underline{u}_a$ and micelle size variations result in an

increment of the interaction energy which is calculated in Appendix B (eqs B1−B3). The total free energy increment is

$$\delta\mathcal{F} = \delta\mathcal{F}_0 + \delta\mathcal{F}_{\text{int}} \simeq C_0\sum_a d_a^{\,2} + C_1\sum_{a,b} u_{\|a,b}^{\,2} + C_2\sum_{a,b} u_{\perp a,b}^{\,2} + C_3\sum_{a,b} u_{\|a,b}(d_a + d_{a,b}) + C_4\sum_{a,b} d_a d_{a+b} \quad (26)$$

where $u_{\|a,b} = (\underline{u}_{a+b} - \underline{u}_a)\cdot\underline{e}_b$, $u_{\perp a,b} = (\underline{u}_{a+b} - \underline{u}_a)\cdot\underline{t}_b$, $\underline{e}_b$ is the unit vector parallel to $\underline{b}$, $\underline{t}_b$ is the unit vector perpendicular to $\underline{b}$, $C_0 = -(\pi/2D^{(0)})\tilde{\lambda} + (3\sigma^2/4D^{(0)})[x^2I_2(x) + 2I_3(x) - 2I(x) - 2xI_1(x)]$, $C_1 = (\sigma^2/2D^{(0)})I_2(x)$, $C_2 = -(\sigma^2/2xD^{(0)})I_1(x)$, $C_3 = -(\sigma^2/2D^{(0)})xI_2(x)$, $C_4 = (\sigma^2/4D^{(0)})(x^2I_2(x) - 2I_3(x))$, and $x = L^{(0)}/D^{(0)}$. The function $I(x)$ is defined in eq 15, $I_1(x) = -(\mathrm{d}I(x)/\mathrm{d}x)$, $I_2(x) = -(\mathrm{d}I_1(x)/\mathrm{d}x)$, and the function $I_3(x)$ is defined in eq B4. The stability analysis can be performed in the standard way: the quadratic form in eq 26 is extended to complex u, d (in analogy with the scalar product) and then the plane-wave distortions with wave-vector $\underline{q}$, $\underline{u}_a = \underline{u}e^{i\underline{q}\cdot\underline{a}}$, $d_a = de^{i\underline{q}\cdot\underline{a}}$, are considered (this is enough due to the translational invariance of the ground state). With $\underline{u} = u\underline{e}_1 + v\underline{t}_1$, we get

$$\begin{aligned}\delta\mathcal{F} = C_0|d|^2 + 2C_1\Big[&(1-\cos q_1)\left|u\right|^2 + \frac{1}{4}(1-\cos q_2)\left|\sqrt{3}v - u\right|^2 + \frac{1}{4}(1-\cos q_3)\left|\sqrt{3}v + u\right|^2\Big] + \\ &2C_2\Big[(1-\cos q_1)\left|v\right|^2 + \frac{1}{4}(1-\cos q_2)\left|\sqrt{3}u - v\right|^2 + \frac{1}{4}(1-\cos q_3)\left|\sqrt{3}u - v\right|^2\Big] - 2C_3\, Im\Big\{\Big[u\sin q_1 + \frac{1}{2}(\sqrt{3}v - u)\sin q_2 - \frac{1}{2}(\sqrt{3}v + u)\sin q_3\Big]d^*\Big\} + \\ &C_4|d|^2(\cos q_1 + \cos q_2 + \cos q_3)\end{aligned}$$

where $q_i = \underline{q}\cdot\underline{b}_i$, $i = 1, 2, 3$, $q_1 + q_2 + q_3 = 0$, *Im* means the imaginary part of a complex number, and d^* is complex conjugate of d. The most dangerous deformation mode is $v = 0$, $q_1 = q$, $q_2 = -q/2$, $q_3 = -q/2$, and $q = 4\pi/3$ (it corresponds to the period $3L^{(0)}$ along the principal directions $\underline{e}_1, \underline{e}_2, \underline{e}_3$). The stability criterion ($\delta\mathcal{F} > 0$) reads

$$\lambda < \lambda^* \equiv 2\sigma^2\left(\frac{3}{4\pi}f(x) + \ln\frac{2D}{r_{\min}} - 2\right) \quad (27)$$

$$f(x) = \frac{x^2}{2}I_2(x) + 3I_3(x) - 2I_0(x) - 2xI_1(x)$$

$f(x)$ rapidly grows as ϕ is increased [$\phi = \pi/(2\sqrt{3}x^2)$]. Alternatively, using eqs 23 and 27, we can consider λ^* as a function of P_s: $\lambda^* = \lambda^*(P_s)$; λ^* is increasing with P_s. Thus, for a given λ, a monodisperse hexagonally ordered system of surface micelles becomes locally stable when the surface pressure P_s exceeds a certain threshold P^* defined by the condition $\lambda^*(P^*) = \lambda$ (or, equivalently, the area fraction of micelles ϕ exceeds ϕ^* corresponding to P^*). This threshold marks the transition from a disordered system of polydisperse micelles to a hexagonal array of more monodisperse micelles (here we assume that thermal fluctuations of micelle positions are sufficiently weak at P^*, i.e., that P^* is higher than P^c considered in section 5.5). A significant increase of the scattering intensity is anticipated at the threshold. Based on the AFM and GISAXS data (refs 7, 8, and 12 and Figures 2 and 3), the threshold is roughly $P_s \sim 0.5$ dyn/cm for F8H16. Using eqs 23 and 27 with $P^* = 0.5$ dyn/cm (note that this P^* is indeed not smaller than P^c calculated in section 5.5) and $P_{12} = -0.25$ (dyne/cm), we get an estimate of the edge tension for F8H16: $\lambda = \lambda^*(P^*) \approx 2.6 \times 10^{-7}$ dyne. Note that in view of eq 24 the critical pressure P^* depends on P_{12} in a simple way: $P^* = P_0^*(\lambda) + P_{12}$, where $P_0^*(\lambda)$ is independent of P_{12}.

7. Discussion and Conclusions

1. In this paper, we consider surface structures formed by the semifluorinated alkane F8H16 (with 8 carbons in the fluorinated block and 16 carbons in the hydrogenated block) at the water/air interface. The theoretical study is focused on large surface micelles and their patterns observed at sufficiently low molecular areas. Micelle formation is normally hinged on two essential factors: (1) a tendency for a phase segregation and (2) an interaction preventing precipitation of the micelles. Regarding the first factor, we produce extensive evidence that the relevant segregation is not a liquid/gas phase separation but rather a liquid/liquid segregation between two different structures of the Langmuir film. Using the AFM images and surface pressure (P_s) vs area per molecule (A) data, we calculate the ratio of the surface densities (inverse areas per molecule) in the phase 1 (inside micelles) and phase 2 (outside): $(c_1/c_2) = (A_2/A_1) \approx 1.3$ (see eq 2). This result essentially excludes a liquid/gas coexistence that would imply a large ratio of the densities.

The liquid/liquid coexistence picture is also supported by the surface potential and X-ray reflectivity measurements[18] (see section 3).

2. As for the second factor, we argue that local interactions cannot do the job of micelle stabilization because the observed micelle diameter is much larger than the molecular length. We therefore consider long-range electrostatic interactions assuming that micelles carry permanent dipole moments. The latter conjecture is justified by the electric surface potential studies[18] that provide the value of the dipole moment per unit area σ (see eq 3). The permanent dipole moment feature is also consistent with the FH monolayer internal structure of phase 1 (inside the micelles) where F blocks are oriented toward air, while H blocks are in contact with water[7,8] (see Figure 5a). The dipole−dipole interactions provide the general mechanism of surface micelle stabilization (see point 8 below).

3. Let us turn to the structure of the matrix outside the micelles (phase 2). It is important that the dipole moment of this surface phase must be practically zero: the surface potential measurements[18] show that for $A > 0.45$ nm^2 the surface potential $U = 0$ with ∼3% precision relative to U at low A (i.e., in phase 1). On the basis of this feature, we propose that FnHm molecules in the matrix are oriented nearly parallel to the air/water interface. This phase (called the P phase) is expected to show a structure of stripes oriented along the film with permanent dipoles at the interfaces between the stripes (see Figure 4a). The thickness (height) $h = h_2$ of the P phase is defined by the balance between the dipole−dipole interactions and the surface tensions at the surfactant/air and surfactant/water interfaces. The argument against the domain FH/HF structure of the low-density phase proposed in ref 18 (see Figure 4b) is considered in Appendix C.

4. Let us consider how does the surface structure formed by FnHm molecules develop as the surface pressure P_s increases starting from $P_s \approx 0$. The process of surface micelle formation crucially depends on the characteristic surface pressure P_{12} corresponding to the equilibrium coexistence of the two surface phases (FH phase = phase 1 and P phase = phase 2).

(i) If $P_{12} > 0$, then the P phase is formed first at very low P_s (which is practically indistinguishable from 0). Next, as surface pressure P_s exceeds P_{12}, the FH micelles nucleate in the P matrix.

The area fraction ϕ and the size of the micelles increases with P_s. The total number of FH micelles saturates when ϕ exceeds a certain critical value ϕ^* corresponding to the onset of the interaction driven micelle stabilization considered in section 6.

(ii) If $P_{12} < 0$ and $|P_{12}|$ is small, $|P_{12}| < P_0^*$, then islands of P phase (surrounded by very dilute surface gas phase) are formed at very low P_s (large area per surfactant molecule, A). The islands grow to a certain size and then transform in the more favorable FH state (with roughly vertical orientation of FnHm molecules rather then horizontal). Small P islands are stable because the edge energy of the P film is lower than that for the FH film. The FH islands grow predominantly by fusion. The direct fusion of large FH islands is suppressed due to their electrostatic repulsion. Then aggregation of FH islands with the residual undergrown P islands is more efficient. The aggregation results in formation of the FH/P microdomain film (see section 5.3); the FH micelles are "wetted" by the P phase in this structure. The FH domains (micelles) form a hexagonal structure as surface pressure exceeds a critical value $P^* = P_0^* + P_{12}$, where P_0^* depends on the FH/P edge tension λ (see section 6). This transition is accompanied by a decrease of the micelle size polydispersity (see point 12 below).

(iii) If $P_{12} < 0$ and $|P_{12}| > P_0^*$, then P^* is formally negative meaning that the microdomain FH/P film is always ordered (if $P_0^* > P_0^c$): FH micelles form a hexagonal lattice even at $P_s \approx 0$.

(iv) Finally, if $P_{12} < 0$ and $|P_{12}|$ is high, then the P phase does not appear at all. The microdomain phase is not stable in this regime. However, the pressure threshold for this to happen is unrealistically high: $|P_{12}|$ must be higher than at least 20 dyn/cm for F8H16 molecules (see section 5.3).

5. It is the second scenario of micelle formation, (ii), that is predicted for F8H16 molecules. At high area per molecule (i.e., at P_s lower than the experimental error of 0.1 dyn/cm) the system separates forming 2 macroscopic phases: dilute phase (a gas of micelles) in coexistence with the continuous FH/P microdomain phase. That sort of structure is shown schematically in Figure 6b. The two macroscopic phases (dilute and dense) are clearly visible in the AFM image, Figure 3, corresponding to $P_s \approx 0$, $A \approx 0.41$ nm^2. The estimated critical parameters for F8H16 molecules are $P_{12} \approx -0.25$ dyn/cm, $P^* \approx 0.5$ dyn/cm.

6. We must expect that P_{12} monotonically changes as a function of block lengths (n, m) of FnHm molecules. It is therefore likely that the scenario of surface micelle formation must switch from the route (i) (considered just above) to (ii) and then to (iii) on variation of n or m (here we assume that P_{12} is more sensitive to the molecular structure than λ).

Thus, the relevant question is: how does P_{12} depend on n or m? There is no unique answer: it depends on how γ^* (see eq 6) changes with n and m. According to eq 6, γ^* does depend on composition of the FnHm molecule (i.e., roughly on n/m). However, γ^* may either increase or decrease with n/m depending on the sign of the difference between $\gamma_{Fa} + \gamma_{Fw}$ and $\gamma_{Ha} + \gamma_{Hw}$. This subtle difference is not known. Let us therefore restrict the question as follows: how does P_{12} change with $n + m$ for a fixed composition (i.e., for $n/m \approx$ const; this condition ensures that $\gamma^* \approx$ const)? Using eqs 4, 9, 10, and 22, we get $P_{12} \approx [(K_1 - K_2 h_2)/(h_1 - h_2)]$, where K_1 and K_2 are constants. It is natural to expect that h_1 is proportional to the molecular length, i.e., to $n + m$. As for h_2, it depends on h_1 according to eq 10 (note that $h = h_2$, $C \propto 1/H$, and $H = h_1$ in this equation). Using the estimate for γ^* obtained just below eq 10, we find that P_{12} is decreasing with $n + m$. Thus, P_{12} is predicted to become more negative for molecules longer than F8H16, but it may turn positive for sufficiently short molecules.

7. The theory developed in the manuscript predicts that typically the F8H16 layer is not homogeneous, but rather involves parts (domains) of both high-density (FH) and low-density (P) phases. This is true even at low surface pressure (high area per F8H16 molecule). The X-ray reflectivity data are consistent with this idea. The reflectivity probes the structure of surface layers in the vertical direction normal to the layers. The spatial resolution of this technique (as defined by the largest measurable wave-vectors) is about 1 nm; that is, it is not enough to unambiguously resolve the height difference between the two phases: $h_1 - h_2 \approx 0.8$ nm according to the theory. Therefore, the available reflectivity data for F8H16 always correspond to a "superposition" of the vertically inhomogeneous electron density of the FH phase and the homogeneous "background" coming from the P phase. As a result, the measured relative contrast between the upper (fluorinated) and the lower (hydrogenated) sublayers must be lower than that in the pure FH phase. This is exactly what was obtained by the reflectivity: compare 46% of electrons in the upper layer (measured at 7 dyn/cm) vs 61% implied by the model of the pure FH phase, Figure 5a (see ref 7 for details).

8. We predict that micelles are arranged in a hexagonal lattice at high enough surface pressure. This regime is defined by two conditions: (1) thermal fluctuations of micelle positions are weak, this is true for $P > P^c$ (see section 5.5), and (2) micelle size polydispersity is low, $P > P^*$ (see section 6). The latter condition ensures that diffusion coalescence (Ostwald ripening) of micelles is suppressed by their electrostatic interactions.

At lower surface pressure, the micelles are disordered and are polydisperse. In the low-pressure regime, the micelle size is expected to somewhat increase in time due to Ostwald ripening. Several GISAXS experiments separated by several hours were performed on a monolayer kept at $P_s \approx 0.5$ dyn/cm.[12] These experiments yield the same scattering curves (the same lattice parameters) indicating that micelle ordering transition occurs at a lower pressure, i.e., that both P^* and P^c are lower than 0.5 dyn/cm.

9. It is important that the existing AFM data may not provide any reliable information about the thickness of the P phase on water surface for the following reasons:

(i) It is expected that the P phase is in the liquid state (its internal microdomain pattern is short-range: a long-range ordered structure of stripes in 2 dimensions is unstable with respect to fluctuations). It is therefore possible that a fraction of this phase is lost during the transfer of the FnHm film onto silicon wafers.

(ii) The AFM tip may not get a sufficient response from the P film if it remains liquid after the transfer onto the silicon.

(iii) The optimal thickness of the P layer and the difference of chemical potentials in P and FH phases may change due to the transfer onto the silicon. The P phase may become destabilized as a result.

10. Let us estimate the equilibrium size D_{eq} of separate (unaggregated) FH islands (this estimate is relevant for $P_{12} < 0$). For simplicity, we consider the dilute regime when the area fraction of islands, ϕ, is small and their interactions are negligible in comparison with their self-energy (this is true for $\phi \lesssim 0.4$). The equilibrium size must correspond to the minimum of the total energy. The total area of the islands is defined by the total number of FnHm molecules. Therefore, D_{eq} corresponds to the minimum of the free energy per unit area, F_0/A_0, where F_0 is defined in eq 17. Thus we get

$$D_{eq} \simeq \frac{r_{min}}{2} \exp\left(3 + \frac{\lambda_{FH}}{2\sigma^2}\right) \quad (28)$$

With $\lambda_{FH} \sim 10^{-6}$ dyne (see section 53 and Appendix A), we get $D_{eq} \sim 10^5$ nm which is much larger than the observed micelle size. The FH islands are therefore not at equilibrium. The size of both isolated FH islands and of FH micelles in the microdomain FH/P phase (formed as a result of aggregation of FH islands) is rather determined by the electrostatic activation energy (the energy barrier for island fusion) considered in section 5.2. The predicted kinetically controlled micelle size (corresponding to the experimental times between 5 min and 10 h) is in the range 24 ÷ 32 nm (see section 5.2), which is in agreement with the experimental data.

11. We show that the measured strong dependence of surface pressure P_s on molecular area A in the region of micelles can be quantitatively explained in terms of the electrostatic repulsion of micelles (see Figure 7).

12. Another important question concerns the micelle size polydispersity. It is natural to expect that micelles whose size is kinetically controlled are polydisperse (due to diffusion coalescence). This is indeed so at low P_s (see Figure 3). However, according to the AFM images of Figure 2, the micelles are rather monodisperse at higher surface pressures. This effect is explained in section 6: it is shown that the electrostatic repulsion between the micelles may serve to suppress the polydispersity. The important parameters are the edge tension (which favors an increase of the polydispersity) and the strength of micelle interactions (which tends to reduce the polydispersity). At high micelle area fractions, $\phi > \phi^*$ (or, equivalently, at high surface pressure, $P_s > P^*$), the second factor wins, and the free energy decreases as the polydispersity drops. Thus, the micelle system is driven toward the monodisperse state. The critical surface pressure for F8H16 molecules is estimated as $P_s = P^* \sim 0.5$ dyn/cm. On the basis of this P^*, we estimate the line tension at the boundary between FH and P phases as $\lambda \approx 2.6 \times 10^{-7}$dyne.

13. The suppression of micelle polydispersity due to repulsive dipole−dipole interactions appears to be a rather general effect. It apparently also explains formation of nearly monodisperse disklike surface micelles of partially fluorinated long-chain acids.[31] Polar heads of these molecules "anchor" the ends of hydrogenated blocks at the water surface thus ensuring a nearly vertical orientation of the molecules leading to a significant mean vertical dipole moment and, therefore, to the electrostatic repulsion of surface micelles (polar heads can also contribute to the overall vertical dipole moment).

14. We would like to stress one general point concerning the electrostatic interactions of micelles: The electrostatic edge energy $\mathcal{F}_e$ (see eq 12) is essentially independent of the dielectric constant of the medium around the dipolar layer: $\mathcal{F}_e$ is proportional to the square of the mean density of the genuine dipole moment (i.e., involving all dipoles, both "permanent" and "induced") which is directly measured by the surface potential.

15. The surface micelles formed by FnHm molecules are not always circular. The observed shapes of surface micelles include: nearly disklike micelles, disks with central holes, elongated micelles, spirals and straight/bent/meander-like ribbons[7,8,10]. The main theoretical prediction is that once disklike micelles are formed they can be stable and monodisperse. It does not matter if the disks are characterized by an internal (spiral) structure or not: a spiral, which is globally circular, can grow continuously like a homogeneous disk. On the other hand, the theory presented in the manuscript does not treat either the spiral internal structure or the structure of ribbons.

What could be the origin of stability of ribbon structures? How about electrostatic dipole/dipole interactions? Equation 28 approximately defines not only the equilibrium size of a disklike micelle but also the equilibrium ribbon width controlled by the electrostatic effects (apart from an unimportant numerical constant). Note that there is no potential barrier for achieving the equilibrium ribbon width (in contrast to the case of disklike micelles): the ribbons can adjust their width by an appropriate change of their length. The electrostatically defined ribbon width (see eq 28 and the discussion around it) is much larger than the observed width (see ref 10). To achieve an agreement one has to assume that the dipole moment of the FH phase is 3 ÷ 5 times higher than that defined in eq 3 based on the surface potential measurements.

Formation of ribbons indicate that the FnHm layer is possibly anisotropic. In the manuscript, we assumed that both F and H fragments are roughly normal to the layer: F blocks are well-oriented, whereas H blocks are in a partially random-coil conformation (see Figure 5a). There is another natural possibility: H blocks can be extended, however, not normal to the layer, but rather at a certain angle to the normal. Based on the measured thickness of the H sublayer,[7,8] this angle must be around 35°. The H sublayer can be then considered as a smectic-C layer (or a 2-dimensional nematic layer; the relevant director is defined by the average orientation of the projection of an H-block onto the plane of the layer). It is natural to expect that near the micelle edge the director must tend to be parallel to it. For a circular micelle, this leads to the director field which is perpendicular to the radius everywhere, thus implying a singularity at the center. This unfavorable singularity can be avoided by creating a hole near the micelle center. That sort of hole can be observed in many high-resolution AFM images (see ref 8 and Figure 3), in particular, for FnHm molecules with longer H-block ($m = 18$, 20). The tendency for the hole formation must be stronger with better orientational order in the H sublayer.

The transition from disklike micelles to elongated and stripe-like micelles can be also attributed to the nematic (smectic C) structure of the lower (H) sublayer of the FH-phase: The nematic field is necessarily distorted in the disklike micelle; the distortion is smaller in elongated micelles and is absent in straight infinite ribbons (we expect that the H-blocks are tilted along the main ribbon axis).

It remains unclear, however, which factors define the observed finite width of the ribbons. An explanation is proposed in ref 10: Both the X-ray reflectivity and the GIXD (grazing-incidence X-ray diffraction) data indicate that the fluorinated blocks are oriented perpendicular to the layer and are tightly packed. The H blocks on the other hand are expected to be tilted as discussed above. Because of the tilt, it is not possible to match the cross-sections of the F and H blocks (crossed by planes parallel to the layer). As a result, the optimum packing of either H or F blocks (or both) must be distorted. As argued in ref 10, this frustration may serve to stabilize the ribbons of finite width.

There are several issues concerning application of these ideas to the experimentally studied FnHm layers:

(i) The argument implicitly assumes that both sublayers (F and H) of the FH phase must be crystalline (or, at least, that the range of positional order in the sublayers is longer than the ribbon

(29) Landau, L. D.; Lifshitz, E. M.; Pitaevskii, L. P. *Physical Kinetics*; Butterworth-Heinemann: London, 1997.

(30) Rabolt J. F.; Russell T. P.; Twieg R. J. *Macromolecules* **1984**, *17*, 2786. Russell T. P.; Rabolt J. F.; Twieg R. J.; Siemens R. L. *Macromolecules* **1986**, *19*, 1135.

(31) Kato T.; Kameyama M.; Ehara M.; Iimura K. *Langmuir* **1998**, *14*, 1786.

width). This is not the case for FnHm layers studied experimentally so far (in particular, for F8H16 and F14H20 investigated in this paper and in ref 10, respectively): for example, the results from GIXD[10] show that the H sublayer is never crystalline, whereas the F sublayer could be sometimes involved in the crystallization but typically also is largely in a liquidlike state. Therefore, the idea hinged on the optimum packing frustration is hardly applicable to the studied FnHm systems: it is hardly possible to anticipate a long-range effect of the packing mismatch in the F and H sublayers with amorphous, liquidlike structure of the H layer involving packing of just a few neighboring CH_2 units. In this case, the packing mismatch results simply in an increase of the interfacial tension between F and H sublayers.

(ii) The argument of ref 10 does not take into account that, although the cross-section of F block is nearly circular, the H block cross-section is flat (trans zigzag). This cross-section anisotropy partially compensates for the packing mismatch if the H blocks are tilted along the short axis of their cross-section.

(iii) The ribbon structure proposed in ref 10 (see model I in Figure 12 in this reference) invites side-by-side aggregation of the ribbons as a result of the van der Waals attraction of the upper fluorinated sublayers. Note that there are no geometrical restrictions opposing merging of the fluorinated sublayers since all of the F blocks are oriented vertically. Thus, a continuous upper F sublayer can be formed, while the lower H sublayer may still show stripes. Is this structure consistent with the SFM images reported in ref 10? This does not seem to be the case in view of considerable height variations across the gaps between the ribbons. A phase-mode AFM study may help to resolve this issue. Most probably, the side-by-side aggregation of ribbons is prevented by their electrostatic repulsion. In this case, the pressure dependence of the gap between the neighboring ribbons may help to assess the strength of this repulsion.

(iv) One may anticipate that the degree of both orientational and positional order in the H sublayer increases with the H block length (note that melting temperatures of bulk solid structures of FnHm increase with *m*, see ref 30). For long enough H blocks, when the positional (crystal-like) order in the H sublayer is long-range enough, the mechanism of ribbon stabilization based on the packing mismatch may become valid. Note however that even in the large *m* regime this mechanism is no more convincing that the electrostatic stabilization of ribbon width: we miss at least a semiquantitative estimate of the optimum ribbon width implied by the packing mismatch (such an estimation does not seem to be an easy task as it would require a consideration of a complicated inhomogeneous distortion of the positional structure in the H sublayer).

One must also bear in mind that both water and solvent molecules can penetrate/remain in the H sublayer thus affecting its structure and, in particular, the tilt angle. Thus, the surface micelle geometry may depend on the solvent used during preparation of the Langmuir layers of FnHm. A very interesting effect of that sort was observed in ref 10: after exposing the layers to a solvent vapor, the straight ribbons turn to meander-like or vice versa depending on the solvent. Larger tilt angle corresponds to a higher energy penalty for inhomogeneous nematic director field leading to a destabilization of bent/meander-like ribbons. It is worth checking if the experimentally observed transitions are indeed accompanied by the anticipated changes of the tilt angle.

In view of the above discussion it would be extremely interesting to assess the role of electrostatics for the size and geometry of FnHm surface micelles. One way to do it is to deposit the FnHm layer not at the interface with bulk water, but rather on top of a thin water layer of thickness h_w. The effect of h_w on the long-range part of electrostatic interactions can be predicted quantitatively; it must be significant for h_w in the range of 10−20 nm. Thus, the experimental question is whether the surface structure significantly depends on h_w or not.

Acknowledgment. We acknowledge stimulating discussions with Michel Goldmann and Mounir Maaloum.

Appendix A: Coalescence Rates: Lifshitz−Slyozov Mechanism vs Fusion

(i) Diffusion of FnHm Molecules in the "Surface Gas" Phase. The saturated surface pressure in the "gas" phase near a curved edge of an island is

$$P \simeq P_\infty + \frac{\lambda}{R}\frac{c_{out}}{c_{in}} \tag{A1}$$

where P_∞ is the saturated surface pressure near a straight edge, $\lambda = \lambda_{FH}$ is the edge tension, R is the radius of curvature, and c_{out} and c_{in} are surface concentrations in the "gas" and in the "condensed" phase, respectively (i.e., $c_{in} = 1/A_1$, where A_1 is the area per molecule in the FH phase, and a similar relation holds for c_{out}). According to the Lifshitz−Slyozov theory,[29] the second term in the rhs of eq A1 sets the amplitude of the concentration variation across the surface gas phase: $\delta c_{out} \sim (1/k_BT)(\lambda/R)(c_{out}/c_{in})$. The typical concentration gradient in the surface gas phase is $\nabla c \sim \delta c_{out}/R$ (here we assume that the fraction ϕ of FH islands is ∼1/2, otherwise the gradient is reduced by the factor $\ln(1/\phi)$), the density of molecular flux is $J = D_{out}\,\nabla c \sim D_{out}(\delta c_{out}/R)$ (here $D_{out} \sim k_BT/6\pi\eta l$ is the diffusion constant of FnHm molecules in the surface gas phase, η is the viscosity of water). The rate of change of the island radius is $dR/dt = J/c_{in}$. Thus, we find that the typical island radius R grows according to the scaling law $R^3 \sim k_1 t$, where

$$\kappa_1 \sim \frac{\lambda}{6\pi\eta l}\frac{c_{out}}{c_{in}^2} \tag{A2}$$

(ii) Fusion. The fusion time is essentially diffusion time between collisions of an island with a neighboring island: $t \sim R^2/D_{isl}$, where $D_{isl} \sim k_BT/6\pi\eta R$ is the island diffusion constant ($6\pi\eta R$ is the Stokes friction coefficient for a rigid sphere of radius R in the bulk of a fluid; for a circular disk moving at the surface the friction coefficient is smaller by a numerical factor which is neglected here). Therefore, $R^3 \sim k_2 t$, where $\kappa_2 \sim k_BT/6\pi\eta$. Therefore $\kappa_1/\kappa_2 \sim (\lambda/k_BTlc_{in})(c_{out}/c_{in}) \ll 1$ since $c_{out}/c_{in} \ll 1$ and $\lambda/k_BTlc_{in} \sim 1$. We estimate the parameters involved as follows: $l \sim 3$ nm, $1/c_{in} \sim 0.5$ nm^2; λ is estimated assuming that the edge is equivalent to a stripe of width ∼1 nm with surface tension ∼20 dyn/cm (the typical value for Teflon): $\lambda \sim 1$ nm × 20 dyn/cm $\sim 2 \times 10^{-6}$ dyne.

To resume, the island growth due to diffusion coalescence is negligible in comparison with the effect of fusion.

Appendix B: Interaction Energy of the Weakly Deformed Hexagonal Array of Micelles

The interaction energy increment is

$$\delta\mathcal{F}_{int} \simeq \delta\mathcal{F}_{int}^{(1)} + \delta\mathcal{F}_{int}^{(2)} \tag{B1}$$

where $\delta\mathcal{F}_{int}^{(1)}$ incorporates formally linear terms (in δL, δD), $\delta\mathcal{F}_{int}^{(2)}$ accounts for the quadratic terms (higher-order terms are omitted)

$$\delta\mathscr{F}_{\text{int}}^{(1)} = \sum_{a,b}\left(\frac{\partial F_{\text{int}}}{\partial L}\delta L + \frac{\partial F_{\text{int}}}{\partial D_1}\delta D_1 + \frac{\partial F_{\text{int}}}{\partial D_2}\delta D_2\right)$$

where $F_{\text{int}} = F_{\text{int}}(L, D_1, D_2)$, the derivatives are taken at $L = L^{(0)}$, $D_1 = D_2 = D^{(0)}$, $\delta L = L_{\text{a, b}} - L^{(0)}$, $\delta D_1 = D_{\text{a}} - D^{(0)} = d_{\text{a}}$, and $\delta D_2 = D_{\text{a + b}} - D^{(0)} = d_{\text{a + b}}$

$$\frac{\partial F_{\text{int}}}{\partial L} = -\sigma^2 I_1(x), \quad \frac{\partial F_{\text{int}}}{\partial D_1} = \frac{\partial F_{\text{int}}}{\partial D_2} = \frac{\sigma^2}{2}[I(x) + xI_1(x)],$$
$$x = L^{(0)}/D^{(0)}$$

The function $I_1(x) = -\mathrm{d}I(x)/\mathrm{d}x$, $I(x)$ is defined in eq 15. Taking into account that $L_{\text{a, b}}{}^2 = [(L^{(0)} + u_{\|a,b})^2 + u_{\perp a,b}{}^2]^{1/2}$ ($u_{\|a,b}$ and $u_{\perp a,b}$ are defined after eq 26) and that

$$\sum_{a,b} u_{\|a,b} = 0, \quad \sum_a d_a = -\frac{1}{2D^{(0)}}\sum_a d_a{}^2$$

(the first condition comes from the requirement that the total film area is constant, the second, from eq 25) we obtain

$$\delta\mathscr{F}_{\text{int}}^{(1)} = -\frac{\sigma^2}{2L^{(0)}}I_1(x)\sum\nolimits_{\text{a, b}} u_{\perp\text{a, b}}{}^2 - \frac{3\sigma^2}{2D^{(0)}}[I(x) + xI_1(x)]\sum_a d_a{}^2 \quad \text{(B2)}$$

The quadratic term reads

$$\delta\mathscr{F}_{\text{int}}^{(2)} = \sum_{a,\,b}\left\{\frac{1}{2}\frac{\partial^2 F_{\text{int}}}{\partial L^2}u_{\|\,a,b}{}^2 + \frac{\partial^2 F_{\text{int}}}{\partial L\partial D_1}u_{\|\,a,b}(d_a + d_{a+b}) + \frac{1}{2}\frac{\partial^2 F_{\text{int}}}{\partial D_1{}^2}(d_a{}^2 + d_{a+b}{}^2) + \frac{\partial^2 F_{\text{int}}}{\partial D_1\partial D_2}d_a d_{a+b}\right\} \quad \text{(B3)}$$

where the symmetry with respect to the permutation $D_1 \rightleftharpoons D_2$ is taken into account, and

$$\frac{\partial^2 F_{\text{int}}}{\partial L^2} = \frac{\sigma^2}{D^{(0)}}I_2(x)$$

$$\frac{\partial^2 F_{\text{int}}}{\partial L\partial D_1} = -\frac{x}{2}\frac{\sigma^2}{D^{(0)}}I_2(x)$$

$$\frac{\partial^2 F_{\text{int}}}{\partial D_1{}^2} = \frac{\sigma^2}{4D^{(0)}}(x^2 I_2(x) + 2I_3(x))$$

$$\frac{\partial^2 F_{\text{int}}}{\partial D_1\partial D_2} = \frac{\sigma^2}{4D^{(0)}}(x^2 I_2(x) - 2I_3(x))$$

Here $I_2(x) = -\mathrm{d}I_1(x)/\mathrm{d}x$ and

$$I_3(x) = -I(x) + \int_{-\pi/2}^{\pi/2} d\alpha \int_0^{\pi/2} d\beta\, \frac{\cos 2\beta \sin^2\beta}{(x^2 + 2x\sin\alpha\cos\beta + \cos^2\beta)^{3/2}}\left[\frac{6x^2\cos^2\alpha}{x^2 + 2x\sin\alpha\cos\beta + \cos^2\beta} - 2\right] \quad \text{(B4)}$$

Appendix C: Analysis of the FH/HF Domain Structure

The surface potential (U) measurements[18,28,24] show that U is always nearly zero for $A > 0.45 \div 0.55$ nm^2, with the precision of about 3% (as compared to the typical surface potential ~1 V in the high-density phase). The areas of FH and HF domains must therefore be equal with a high precision. However, there is no symmetry to provide that sort of balance. On the contrary, the free energies (per unit area) of the FH and HF domains are different: the HF domain is less favorable as it implies that H blocks are in contact with air and F blocks face water. The free energy difference $\Delta\gamma$ amounts at least to the difference between the F/air and H/air surface tensions, i.e., between surface tensions of polyethylene and Teflon, $\Delta\gamma \gtrsim \gamma_{\text{Ha}} - \gamma_{\text{Fa}} \approx 13$ dyn/cm.[25]

The domain width w (Figure 4b) is defined by the balance between the domain edge energy (the local energy of interfaces between the domains) $\mathscr{F}_0$ and the electrostatic energy of dipole interactions $\mathscr{F}_{\text{e}}$ (more precisely, the edge contribution to the electrostatic energy): $\mathscr{F} = \mathscr{F}_0 + \mathscr{F}_{\text{e}}$. Note that the equilibrium micelle size is defined by the same mechanism (see section 7). Note also that $\mathscr{F}_0$ is the bare edge energy that does not include electrostatic interactions (apart from local interactions with the range $r < r_{\min}$). Obviously $\mathscr{F}_0 \simeq \lambda_0\mathscr{A}/w$, where λ_0 is the bare line tension at the FH/HF interface and $\mathscr{A}$ is the total area of the structure. The electrostatic energy is obtained in the logarithmic approximation using the first eq 12:

$$\mathscr{F}_{\text{e}} \simeq -8\sigma_0{}^2\frac{\mathscr{A}}{w}\ln\frac{w}{r_{\min}}$$

Minimizing $\mathscr{F} = \mathscr{F}_0 + \mathscr{F}_{\text{e}}$ with respect to w

$$w \sim r_{\min}\exp\left(\frac{\lambda_0}{8\sigma_0{}^2} + 1\right)$$

The FH/HF interface of height $h \sim 3$ nm is characterized by the surface tension $\gamma_{\text{FH}} > 20$ dyn/cm (see end of section 4.1). Therefore, $\lambda_0 \sim \gamma_{\text{FH}}h \gtrsim 6 \times 10^{-6}$ dyne. On using also eq 3 we obtain $w \gtrsim 4 \times 10^5$ nm. Decreasing $r_{\min}$ from 1 nm (the accepted value) to 0.3 nm (the expected width of the dipole layer) does not make any qualitative difference: it is clear that w is necessarily large, $w \gg 10$ nm (this condition stays valid even if γ_{FH} is decreased by a factor of 4).

Further, let us allow for an asymmetry: each FH stripe of width $w_1 = w(1 + \epsilon)$, each HF stripe of width $w_2 = w(1 - \epsilon)$. The number and the energy of FH/HF interfaces are independent of ϵ, but the energy F_i of the surfactant/water and surfactant/air interfaces does depend on ϵ

$$F_i = \text{const} - 2\Delta\gamma w\epsilon$$

where F_i is the interfacial free energy per two neighboring stripes (FH and HF) and per unit length along the stripe. An increase of ϵ driven by $\Delta\gamma$ is opposed by the dipole−dipole interactions. The electrostatic energy is defined in the first eq 12, $\mathscr{F}_{\text{e}} \simeq -\int\{\nabla\sigma(r_1)\cdot\nabla\sigma(r_2)/r_{12}\}\, d^2r_1 d^2r_2$, where r_{12} is the distance between r_1 and r_2 and σ is the dipole moment per unit area. This equation is valid since $w \gg h$. We assume that $\sigma = -\sigma_0$ in the FH domains and $\sigma = \sigma_0$ in the HF domains, with $\sigma_0 \approx 2.4 \times 10^{-4}$ CGS (see eq 3). $\mathscr{F}_{\text{e}}$ can then be simplified as

$$\mathscr{F}_{\text{e}} \simeq -4\sigma_0{}^2\sum_{n,m}(-1)^{n-m}\int\frac{\mathrm{d}y_n\mathrm{d}y_m}{r_{nm}} + \text{const}$$

where n and m count all interfaces between FH and HF domains (each interface is considered as a line in the y-direction parallel to the stripes) and r_{nm} is the distance between two points on the lines n and m, $n \neq m$. The electrostatic energy per two neighboring stripes and per unit length along the stripe is

$$F_e \simeq 16\sigma_0^2 \sum_m (-1)^{n-m} \ln d_{nm} + \text{const}$$

where $m \neq n$ and d_{nm} is the distance between lines n and m. Treating ϵ as a small parameter we get in the quadratic approximation

$$F_e \simeq 2\pi^2 \sigma_0^2 \epsilon^2 + \text{const}$$

Minimizing $F_e + F_i$ with respect to ϵ results in

$$\epsilon \simeq \frac{\Delta\gamma w}{2\pi^2 \sigma_0^2}$$

With $\Delta\gamma \sim 10$ dyn/cm, $w \sim 10$ nm, we thus obtain $\epsilon \sim 1$ (for $w \gg 10$ nm the predicted asymmetry is strong: $\epsilon \simeq 1$). The predicted ϵ is thus much higher than the experimental bound, $\epsilon \sim 0.03$. This large discrepancy means that the FH/HF domain structure is not realistic.

LA060638+